MOLECULAR AND CELLULAR BIOLOGY, Sept. 1997, p. 5001–5015 Vol. 17, No. 9
0270-7306/97/$04.00+0

Saccharomyces cerevisiae Nip7p Is Required for Efficient 60S Ribosome Subunit Biogenesis

NILSON I. T. ZANCHIN,[1] PAUL ROBERTS,[1] ARAVINDA DESILVA,[1] FRED SHERMAN,[2] AND DAVID S. GOLDFARB[1]*

Department of Biology, University of Rochester, Rochester, New York 14627,[1] and Department of Biochemistry and Biophysics, University of Rochester, Rochester, New York 14642[2]

Received 14 November 1996/Returned for modification 12 December 1996/Accepted 2 June 1997

The *Saccharomyces cerevisiae* temperature-sensitive (ts) allele *nip7-1* exhibits phenotypes associated with defects in the translation apparatus, including hypersensitivity to paromomycin and accumulation of halfmer polysomes. The cloned *NIP7*$^+$ gene complemented the *nip7-1* ts growth defect, the paromomycin hypersensitivity, and the halfmer defect. *NIP7* encodes a 181-amino-acid protein (21 kDa) with homology to predicted products of open reading frames from humans, *Caenorhabditis elegans*, and *Arabidopsis thaliana*, indicating that Nip7p function is evolutionarily conserved. Gene disruption analysis demonstrated that *NIP7* is essential for growth. A fraction of Nip7p cosedimented through sucrose gradients with free 60S ribosomal subunits but not with 80S monosomes or polysomal ribosomes, indicating that it is not a ribosomal protein. Nip7p was found evenly distributed throughout the cytoplasm and nucleus by indirect immunofluorescence; however, in vivo localization of a Nip7p-green fluorescent protein fusion protein revealed that a significant amount of Nip7p is present inside the nucleus, most probably in the nucleolus. Depletion of Nip7-1p resulted in a decrease in protein synthesis rates, accumulation of halfmers, reduced levels of 60S subunits, and, ultimately, cessation of growth. Nip7-1p-depleted cells showed defective pre-rRNA processing, including accumulation of the 35S rRNA precursor, presence of a 23S aberrant precursor, decreased 20S pre-rRNA levels, and accumulation of 27S pre-rRNA. Delayed processing of 27S pre-rRNA appeared to be the cause of reduced synthesis of 25S rRNA relative to 18S rRNA, which may be responsible for the deficit of 60S subunits in these cells.

Eukaryotic ribosome biogenesis takes place mainly in the nucleolus, where approximately 80 ribosomal proteins (rproteins) and 4 rRNAs assemble into 40S and 60S subunits (reviewed in reference 66). In eukaryotes, synthesis of rRNAs is not achieved by transcription of the individual species. Instead, three of the four rRNAs (18S, 5.8S, and 25 to 28S) are produced from a single RNA polymerase I transcript (35S in yeast), which, in addition to the mature rRNAs, contains two external transcribed spacers, the 5′ ETS and 3′ ETS, and two internal transcribed spacers, ITS1 and ITS2 (66). The 35S pre-rRNA, which is covalently modified by methylation and pseudouridinylation, serves as a template onto which a number of rproteins and non-rproteins associate and is processed by endo- and exonucleases. The fourth rRNA species (5S) is transcribed independently by RNA polymerase III (66). Following assembly in the nucleolus, ribosomal subunits are selectively exported to the cytoplasm (39).

Ribosome biogenesis has been studied in many eukaryotic organisms but is best characterized in *Saccharomyces cerevisiae*. In yeast, although the level of total rproteins changes during various stages of growth, stoichiometric ratios of 40S rproteins and 60S rproteins are independently maintained. Intrasubunit stoichiometry is maintained primarily by the coordinate transcription of rprotein genes (38, 66) and by the turnover of rproteins that are expressed in excess (10, 30, 61). Therefore, the depletion or mutation of individual rprotein genes can result in the decrease of cellular levels of 40S or 60S subunits, which can lead to imbalances in the 40S/60S subunit ratio (8, 32, 33, 44). Imbalances between 40S and 60S subunits can also result from the depletion or mutation of non-rprotein factors involved in rRNA processing and ribosome assembly (16, 26, 42, 46, 55, 65).

Ribosome assembly is not well characterized. Pulse-labeling analysis indicated that a group of rproteins assembles early on the pre-rRNA, while another group assembles late on the mature rRNA (23). Early experiments suggested that 40S subunits undergo maturation steps in the cytoplasm, which include processing of 20S pre-rRNA to 18S rRNA (62). Evidence supporting ribosome assembly reactions in the cytoplasm was also reported by Tollervey et al. (59), who showed that newly synthesized 18S and 25S rRNAs are associated with cytoplasmic particles with sucrose gradient mobilities lower than those of 40S and 60S mature subunits.

For yeast, the processing steps that convert 35S pre-rRNA into mature rRNAs are relatively well understood (reviewed in reference 57; see also Fig. 9). The 35S pre-rRNA is initially cleaved at sites A_0, A_1, and A_2, yielding the 20S pre-rRNA and the $27SA_2$ pre-rRNA. The 20S pre-rRNA is subsequently converted to 18S rRNA after processing at site D. Synthesis of 18S rRNA has been studied in most detail and requires a number of *trans*-acting factors, including small nucleolar RNAs (snoRNAs) U3, U14, snR10, and snR30 (17, 27, 34, 56), snoRNA-interacting proteins Nop1p, Sof1p, and Gar1p (12, 19, 58), RNA methylase Dim1p (25), putative RNA helicase Rrp3p (36), and nucleolar proteins Nsr1p and Rrp5p (21, 22, 26, 63).

The $27SA_2$ pre-rRNA is processed into mature 5.8S and 25S rRNAs by two alternative pathways. The major pathway involves cleavage at site A_3 by RNase MRP (6, 29, 48), followed by 5′-3′ exonuclease digestion to site $B1_S$, yielding the $27SB_S$ pre-rRNA. In the minor pathway, the $27SB_L$ pre-rRNA is generated by processing at site $B1_L$. Subsequently, both the $27SB_S$ and $27SB_L$ pre-rRNAs are processed identically in

* Corresponding author. Mailing address: Department of Biology, University of Rochester, Rochester, NY 14627. Phone: (716) 275-3890. Fax: (716) 275-2070.

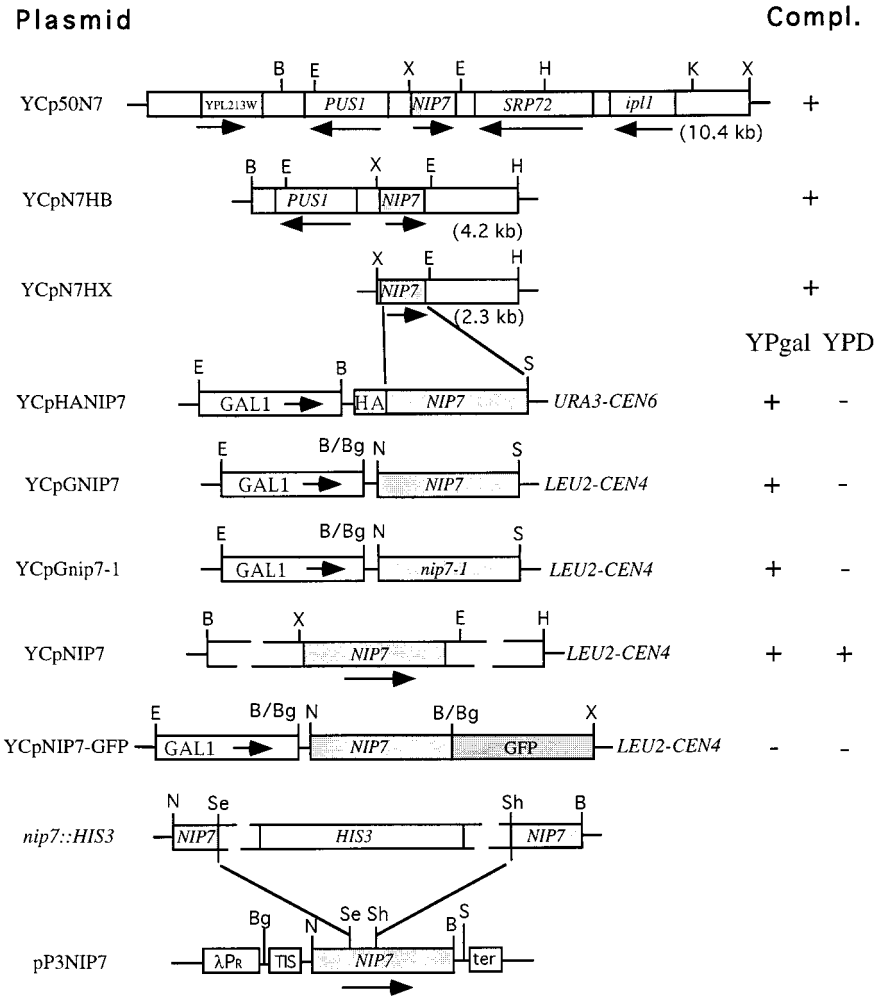

FIG. 1. Restriction maps of the plasmids used in this study. Complementation (Compl.) of the *nip7-1* temperature sensitivity and of *nip7::HIS3* disruption is shown on the right. +, plasmid was able to support growth on agar plates, producing visible colonies after a 2- to 3-day incubation. The DNA sequence flanking *NIP7* was obtained from the *Saccharomyces* Genome Data Base. The directions of the promoters and relevant restriction enzyme sites are shown. Restriction enzyme abbreviations: B, *Bam*HI; Bg, *Bgl*II; E, *Eco*RI; H, *Hin*dIII; K, *Kpn*I; N, *Nde*I; S, *Sal*I; Se, *Spe*I; Sh, *Sph*I; X, *Xba*I. λP_R, TIS, and ter in pP3NIP7 correspond, respectively, to the phage λ p_R promoter, to the translation initiation sequence from the *E. coli atpB* gene, and to the phage fd transcription terminator.

ITS2, producing the 25S rRNA and, respectively, $5.8S_S$ and $5.8S_L$ rRNAs. Processing of the $5.8S_S$ rRNA 5′ end requires the function of the exonucleases Xrn1p and Rat1p (15, 54). Two other exonucleases, Rrp4 and RNase P, are involved in 5.8S rRNA 3′ end formation (5, 31). Although our understanding of 25S rRNA maturation is incomplete, the putative RNA helicases Sbp4p, Drs1p, and Dbp3p (42, 46, 65) and the nucleolar proteins Nop2p and Nop4p/Nop77 (3, 16, 55) were shown to function specifically in 60S biogenesis. Inactivation or depletion of any of these proteins impaired processing of the 27S pre-rRNA.

This study describes the identification and functional analysis of the novel *S. cerevisiae* gene *NIP7. NIP7* is essential in yeast and well conserved among eukaryotes, but it does not contain recognizable protein sequence motifs or show similarity to other known proteins. The depletion of Nip7-1p resulted in decreased protein synthesis rates, reduced levels of 60S subunits, and defects in pre-rRNA processing, especially that of 27S pre-rRNA. These phenotypes are consistent with a role for Nip7p in 60S ribosome biogenesis.

MATERIALS AND METHODS

DNA analysis, yeast genetic techniques, and media. DNA cloning and electrophoresis analysis were performed as described by Sambrook et al. (47). DNA sequencing was performed by the Sequenase method (United States Biochemical). Growth and genetic analysis of yeast strains were performed as described by Sherman et al. (50, 51). Various carbon sources were added to yeast extract-peptone (YP) and synthetic complete (SC) media. YPD and SCglu media contained 2% glucose as a carbon source, and YPgal and SCgal contained 1% galactose plus 1% raffinose as a carbon source. A yeast genomic DNA bank (43) was acquired from the American Type Culture Collection (ATCC 37415). The paromomycin sensitivity assay was performed as follows: 100 μl of a cell suspension (optical density at 600 nm [OD_{600}] = 0.1) was spread on YPD plates; then sterile filter disks (Schleicher & Schuell no. 740-E) containing 10, 2 or 0.4 mg of paromomycin sulfate were placed on each plate, and the plates were incubated at 30°C for 2 days. Amino acid sequences were aligned by using the Pileup program from the Genetics Computer Group package (9).

Plasmids and yeast strains. Plasmids used in this study are shown in Fig. 1. YCpNIP7 was constructed by transferring a 4.6-kb DNA fragment (*Hin*dIII-*Bam*HI), containing the wild-type *NIP7* gene with its original promoter and terminator, in the vector YCplac111 (11). In order to construct an HA-tagged Nip7 protein, a DNA sequence encoding three repeats of the influenza virus hemagglutinin antigen epitope (HA) was fused with the DNA sequence corresponding to the N terminus of the *NIP7* open reading frame (ORF). The HA-*NIP7* fusion was then placed under the control of the *GAL1* promoter in pRS316-GAL1 (28), generating YCpHANIP7. YCpGNIP7 contains the wild-

TABLE 1. *S. cerevisiae* strains

Strain[a]	Genotype
W303-1a[b]	*MAT***a** *ade2-1 leu2-3,112 his3-11,15 trp1-1 ura3-1 can1-100*
W303α[c]	*MAT*α *ade2-1 leu2-3,112 his3-11,15 trp1-1 ura3-1 can1-100*
DG17	*MAT*α *cyc7-67 leu2-3,112 his3-d1 cyh2R ura3-52*
DG115	*MAT***a** *CYC1-NLS cyc7-67 lys5-10 ura3-52*
DG130	*MAT***a** *CYC1-NLS cyc7-67 lys5-10 ura3-52 nip7-1*
DG438	*MAT*α *cyc7-67 leu2-3,112 his3-d1 cyh2r ura3-52 nip7::HIS3* p[*URA3 ARSH4 GAL1::*HA-*NIP7*]
DG439	*MAT*α *ade2-1 leu2-3,112 trp1-1 ura3-1 nip7::HIS3* p[*URA3 ARSH4 GAL1::*HA-*NIP7*]
DG440	*MAT*α *ade2-1 leu2-3,112 trp1-1 ura3-1 nip7::HIS3* p[*LEU2 ARS1 NIP7*]
DG441	*MAT*α *ade2-1 leu2-3,112 trp1-1 ura3-1 nip7::HIS3* p[*LEU2 ARS1 GAL1::NIP7*]
DG442	*MAT*α *ade2-1 leu2-3,112 trp1-1 ura3-1 nip7::HIS3* p[*LEU2 ARS1 GAL1::nip7-1*]
DG443	*MAT***a**/*MAT*α *ade2-1/ADE2 leu2-3,112/leu2-3,112 his3-11,15/his3-11,15 trp1-1/TRP1 can1-100/CAN1 ura3-1/ura3-52 CYC7/cyc7-67 CYH2/cyh2R NIP7/nip7::HIS3*

[a] Strain DG115 is described in reference 13. All other strains are described in this work.
[b] A gift from M. Nomura.
[c] A gift from S. Wente.

type *NIP7* gene placed under the control of the *GAL1* promoter. This plasmid was constructed by ligating the vector YCplac111 digested with *Eco*RI and *Sal*I, the *GAL1* promoter digested with *Eco*RI and *Bam*HI (isolated from pRS316-GAL1), and the *NIP7* gene digested with *Bgl*II and *Sal*I (isolated from pP3NIP7 [see below]). YCpGnip7-1 carries the temperature-sensitive (ts) *nip7-1* allele, which was amplified by PCR from genomic DNA isolated from strain DG130. The *nip7-1* allele was first inserted between the *Nde*I and *Bam*HI sites of pCYTEXP3 (49). Subsequently, it was inserted in the YCplac111 plasmid, under control of the *GAL1* promoter, by the same strategy used to construct YCpGNIP7. In order to construct a Nip7p-green fluorescent protein (Nip7p-GFP) fusion protein, a *Bam*HI restriction site was created in the vector YCpGNIP7 at the 3′ end of the *NIP7* coding region by PCR. Subsequently, an *Eco*RI-*Bam*HI DNA fragment containing the *GAL1* promoter and the *NIP7* coding region was excised from YCpGNIP7 and ligated with a *Bgl*II-*Xba*I DNA fragment containing the GFP into the vector YCplac111 digested with *Eco*RI and *Xba*I, generating plasmid YCpNIP7-GFP. Expression of *NIP7* in *Escherichia coli* was achieved by using the expression vector pCYTEXP3 (49). The *NIP7* ORF was amplified by PCR, digested with *Nde*I and *Bam*HI, and inserted in the *Nde*I and *Bam*HI sites of pCYTEXP3, generating plasmid pP3NIP7. A *nip7::HIS3* null allele was constructed by removing an internal fragment (*Spe*I-*Sph*I) of the *NIP7* ORF and inserting the *HIS3* genetic marker, producing plasmid pP3nip7::HIS3.

S. cerevisiae strains used in this study are listed in Table 1. DG115 (formerly B-8106) is the parental strain used to isolate the *nip* mutants (13). DG130 is the ts *nip7-1* strain which was used to clone the wild-type *NIP7* gene. DG17 was used to construct a mutant strain conditional for galactose, generating DG438 (see Results). DG439 was generated by three sequential backcrosses of DG438 and either W303-1a or W303α in order to obtain a genetic background similar to W303. DG440, DG441, and DG442 were generated by transforming DG439 with the plasmids YCpNIP7, YCpGNIP7, and YCpGnip7-1, respectively, and eliminating the endogenous YCpHANIP7 by plasmid shuffling. DG443 is a diploid which resulted from a cross between DG438 and W303-1a.

Purification of recombinant Nip7 protein and antiserum production. High levels of Nip7p expression in *E. coli* DH5α were achieved by using plasmid pP3NIP7. In this vector, *NIP7* is under the control of the phage λ p_r promoter, which is induced by shifting *E. coli* cells from 30 to 42°C (2, 49). After a 2-h induction, Nip7p was found in inclusion bodies, which were isolated as described previously (47), and solubilized in a buffer containing 20 mM HEPES-KOH (pH 7.4), 2% Triton X-100, 0.2 mM EDTA, 6 M guanidine hydrochloride, and 250 mM dithiothreitol (DTT) at 50°C for 2 h. The solution was allowed to cool to room temperature and diluted with 1 volume of buffer A (20 mM Tris-Cl [pH 7.4], 100 mM KCl, 1 mM DTT, 0.5 mM EDTA, 10% glycerol). The protein suspension was dialyzed against buffer A, and the insoluble material was removed by centrifugation. Although the supernatant contained relatively pure Nip7 protein, Nip7p was purified further by chromatography with a cation-exchanger resin (Bio-Rex; Bio-Rad). The supernatant was loaded onto a 20-ml column preequilibrated with buffer A, and the column was eluted with a 0 to 50% gradient of buffer B (buffer A containing 1 M KCl) over 80 min with a flow rate of 1 ml/min by using an automated chromatography system (Econo System; Bio-Rad). Concentrated and about 99% pure Nip7p eluted from the column at KCl concentrations of between 220 and 250 mM. Fractions containing Nip7p were pooled and dialyzed against phosphate-buffered saline (47). Rabbit polyclonal antiserum against purified recombinant Nip7p was produced by Pocono Rabbit Farm and Laboratory, Inc. (Canadensis, Pa.).

SDS-PAGE and immunoblot analysis. Proteins were analyzed by sodium dodecyl sulfate–13.5% polyacrylamide gel electrophoresis (SDS–13.5% PAGE) (24). Following SDS-PAGE, proteins were electroblotted to an Immobilon-P membrane (Millipore) at 100 V for 1 h (60), using a Mini Trans-Blot transfer apparatus (Bio-Rad). The Western blot transfer buffer contained 25 mM Tris base, 192 mM glycine, and 15% methanol. Membranes were blocked with 5% bovine serum albumin in TST buffer (20 mM Tris-Cl [pH 8.0], 150 mM NaCl, and 0.05% [vol/vol] Tween 20) and then probed with rabbit polyclonal antiserum raised against Nip7p or eIF-2α (kindly provided by John McCarthy) or with mouse monoclonal antibodies directed against Tcm1p (kindly provided by Jonathan Warner) and Nop1p (kindly provided by John Aris). Subsequently, the blots were incubated with alkaline phosphatase-conjugated anti-rabbit or anti-mouse immunoglobulin G (IgG) and visualized by using 5-bromo-4-chloro-3-indolylphosphate and nitroblue tetrazolium as previously described (47).

Growth curves and analysis of Nip7p depletion. Growth rates of strains DG440, DG441, and DG442 in YPgal and YPD cultures were analyzed as follows. Cultures were inoculated in 40 ml of YPgal and incubated to an OD_{600} of about 0.3. Subsequently, cultures were divided into two fractions, and cells were harvested by centrifugation and resuspended in 100 ml of either YPD or YPgal. Cultures were incubated at 30°C, and the OD_{600} was determined at various time points. In order to keep cultures in exponential growth, they were diluted in fresh medium whenever the OD_{600} reached 0.8. Samples (10 ml) were collected from YPD cultures at various times for the analysis of Nip7p depletion. For isolation of cell extracts, cells were harvested by centrifugation, resuspended in 200 μl of breaking buffer {20 mM HEPES-KOH [pH 7.4], 2 mM magnesium acetate [$Mg(OAc)_2$], 100 mM KCl, 1 mM DTT, 0.5 mM EDTA, 1 mM phenylmethylsulfonyl fluoride [PMSF]}, and disrupted by vortexing in the presence of 1 volume of glass beads. Cell extracts were cleared by centrifugation, and Nip7p was analyzed by SDS-PAGE and immunoblotting.

Measurement of [^{35}S]methionine incorporation. Protein synthesis rates were determined by pulse-chase labeling of total cell protein with [^{35}S]methionine. Strains DG440 and DG442 were incubated at 30°C in SCgal medium lacking methionine until an OD_{600} of about 0.3 was reached. Cells were harvested, resuspended in SCglu lacking methionine, and incubated at 30°C. At various time points, samples from each culture were removed and incubated with 20 μCi of [^{35}S]methionine (DuPont-NEN) per ml at 30°C for 5 min. Unlabeled methionine was then added to a final concentration of 10 mM. Cells were immediately transferred to an ice bath and lysed with 0.2 M NaOH and 0.85% β-mercaptoethanol. Proteins were precipitated with 10% trichloroacetic acid (TCA) as described previously (47) and resuspended in 200 μl of 50 mM Tris-Cl (pH 6.8)–1% SDS. Proteins were extracted by incubation at 95°C for 5 min, and the radioactivity was quantified by liquid scintillation counting.

Pulse-chase labeling of rRNA and Northern analysis. The protocol for metabolic labeling of rRNA was adapted from that of Sun and Woolford (55). Exponentially growing cultures of DG440 (*NIP7*) and DG442 (*GAL::nip7-1*) were shifted from SCgal to SCglu supplemented with uracil (20 μg/ml) and incubated at 30°C for 4 h. Cultures were then divided into two fractions for pulse-chase labeling with either [^{3}H]uracil or [*methyl*-^{3}H]methionine (DuPont-NEN). For labeling with [^{3}H]uracil, cells were harvested by centrifugation, resuspended in fresh SCglu lacking uracil, pulse-labeled for 3 min at 30°C with 50 μCi of [^{3}H]uracil per ml, and chased for up to 1 h after addition of unlabeled uracil to a final concentration of 300 μg/ml. At various times, samples were taken and quickly frozen in a dry ice-ethanol bath. A similar procedure was used to label rRNA with [*methyl*-^{3}H]methionine except that the cells were resuspended in SCglu lacking methionine. Cells were pulse-labeled with 100 μCi of [*methyl*-^{3}H]methionine per ml for 2 min and chased with 100 μg of unlabeled methionine per ml. Total RNA was isolated from yeast cells by the hot-phenol method (20). Small RNA molecules were analyzed by using 6% polyacrylamide gels containing 8.2 M urea. Polyacrylamide gels were fixed in 30% methanol–10% acetic acid for 1 h, incubated in En^{3}Hance (DuPont-NEN), dried, and subjected to autoradiography. Large RNA molecules were separated by electrophoresis on 1.2% agarose–6% formaldehyde gels, transferred by Northern blotting to Hybond nylon

TABLE 2. Paromomycin sensitivity

Paromomycin (mg)	Sensitivity[a]	
	DG115 (*NIP7*)	DG130 (*nip7-1*)
0.4	0	4
2.0	3	8
10.0	3	12

[a] Results are reported as the radius (in millimeters) of clearing around filter discs impregnated with paromomycin as described in Materials and Methods

membranes (Amersham) as described previously (47), and subjected to autoradiography.

For analysis of pre-rRNA steady-state levels, RNA was isolated from strains DG440 (*NIP7*) and DG442 (*GAL::nip7-1*) incubated in YPgal or shifted to YPD. Samples were collected for RNA extraction at time zero and 12 h after the shift to YPD for DG440 and at time zero and 4, 8, and 12 h after the shift to YPD for DG442. RNA was separated by electrophoresis on agarose-formaldehyde gels and transferred by Northern blotting to nylon membranes as described above. Membranes were probed with ^{32}P-labeled oligonucleotides complementary to regions of rRNAs by using the hybridization conditions described by Tollervey (56). The oligonucleotides used (see also Fig. 9) were 5′GGTCTCTCTGCTGC CGGAAATG3′ (probe A), 5′GCTCTCATGCTCTTGCCAAAAC3′ (probe B), 5′TGTTACCTCTGGGCCCCG3′ (probe C), 5′CGTATCGCATTTCGCTGCG TTC3′ (probe D), 5′GGCCAGCAATTTCAAGTTAAC3′ (probe E), and 5′G TTCGCCTAGACGCTCTCTTC3′ (probe F).

Polysome profile analysis and isolation of ribosomal subunits. Standard polysome profile analysis was performed by a protocol adapted from that of Proweller and Butler (40). Cell extracts were isolated from 300-ml cultures grown to mid-exponential phase. Following addition of 3 ml of cycloheximide (10 mg/ml) to the cultures, cells were harvested by centrifugation and resuspended in 0.5 ml of breaking buffer [20 mM HEPES-KOH (pH 7.4), 2 mM $Mg(OAc)_2$, 100 mM KCl, 1 mM DTT, 1 mM PMSF, 100 μg of cycloheximide per ml]. One volume of glass beads was added, the cells were disrupted by vortexing eight times for 20 s, and extracts were cleared by centrifugation at 8,000 × *g* for 5 min. Totals of 20 OD_{254} units were loaded onto 12-ml linear sucrose gradients prepared in polysome buffer [10 mM Tris-Cl (pH 7.4), 70 mM $NH_4(OAc)$, 4 mM $Mg(OAc)_2$]. Polysomes were separated by centrifugation at 40,000 rpm for 4 h at 4°C with a Beckman SW41 rotor. Gradients were fractionated with a Buchler Auto-densiflow IIC fractionator and monitored at 254 nm with a UA-5 Absorbance/Fluorescence monitor (ISCO). For immunoblotting analysis, proteins were precipitated with 10% TCA as described previously (47) and resuspended in protein sample buffer (24). Polysome profile analyses with different KCl concentrations were performed as described for the standard polysome profile analysis except that the breaking buffer contained 20 mM HEPES-KOH (pH 7.4), 3 mM $Mg(OAc)_2$, 10 mM KCl, 1 mM DTT, and 1 mM PMSF and the polysome buffer contained 10 mM Tris-Cl (pH 7.4), 4 mM $Mg(OAc)_2$, and 10 mM KCl. The KCl concentration in both breaking and polysome buffers was increased to 100, 250, or 500 mM, as indicated.

Ribosomal subunits were isolated from mid-exponential-phase cultures by a protocol adapted from the method described by Raué et al. (41). A 4-h Nip7p depletion period prior to ribosome isolation was performed as described for the growth experiments. Cell extracts were prepared in buffer A (20 mM Tris-Cl [pH 7.4], 16 mM $MgCl_2$, 50 mM KCl, 1 mM DTT, 0.2 mM EDTA, 1 mM PMSF) as described above and cleared by centrifugation with a Beckman TLS-55 rotor at 15,000 rpm for 15 min in a Beckman TL-100 ultracentrifuge. Four hundred microliters of the supernatant was layered on 1.6 ml of a 0.5 M sucrose cushion in buffer A and centrifuged at 50,000 rpm for 2.5 h with a Beckman TLS-55 rotor. Ribosomal pellets were resuspended in 200 μl of buffer A. Ribosome dissociation was achieved by adding 200 μl of 2× dissociation buffer (1× dissociation buffer contains 20 mM Tris-Cl [pH 7.4], 16 mM $MgCl_2$, 1 M KCl, 12 mM β-mercaptoethanol, and 0.2 mM EDTA) to the suspension, which was incubated overnight on ice. Insoluble material was pelleted by centrifugation at 14,000 rpm for 5 min in a Microfuge at 4°C. Eight OD_{254} units was loaded on 12-ml linear sucrose gradients prepared in 1× dissociation buffer. Gradient centrifugation and fractionation was performed as described for standard polysome profile analysis.

Immunofluorescence analysis, subcellular fractionation of yeast cells, and NIP7-GFP fusion. Yeast cells were prepared for immunofluorescence essentially as previously described (13). Rabbit polyclonal antiserum raised against Nip7p was incubated with fixed and permeabilized cells overnight at room temperature, using a 1:3,000 dilution. Subsequently, the cells were incubated with fluorescein-conjugated goat anti-rabbit IgG for 6 h at room temperature. Nuclei were stained with 4′,6-diamino-2-phenylindole (DAPI) (1 μg/ml). For subcellular fractionation, nuclei were separated from cytoplasmic fractions by using sucrose step gradients (18). Proteins of the subcellular fractions were precipitated with 10% TCA and analyzed by SDS-PAGE and immunoblotting as described above. The subcellular localization of Nip7p was also analyzed by monitoring the fluorescent signal produced by a fusion of GFP to the carboxy terminus of Nip7p. The Nip7p-GFP fusion protein was expressed by plasmid YCpNIP7-GFP (Fig. 1) transformed into strain W303-1a. Plasmid pDN291 (35) expressing GFP was used as a control.

RESULTS

Cloning of the *NIP7* gene. The ts allele *nip7-1* was isolated with the genetic screen described by Gu et al. (13) and initially analyzed in strain DG130. *nip7-1* cells were hypersensitive to paromomycin (Table 2), an aminoglycoside antibiotic known to interfere with translation (7, 37, 53), and accumulated halfmer-containing polysomes (14) at both permissive (28°C) and nonpermissive (37°C) temperatures (Fig. 2). Both paromomycin sensitivity and halfmer accumulation cosegregated with the ts growth defect in tetrad analysis (data not shown). The *NIP7*$^+$ gene was cloned by complementing the *nip7-1* ts growth defect with a yeast genomic DNA bank (43). Sequence and database analyses revealed that the 10.4-kb insert in the complementing plasmid YCp50N7 (Fig. 1) contained five ORFs located on chromosome XVI. The ORF YPL211W was sufficient to complement both the *nip7-1* ts growth defect and the halfmer defect (Fig. 1 and 2). YPL211W, named *NIP7*, was placed under the control of the *GAL1* promoter of pRS316 (28) to generate YCpHANIP7. As expected, *nip7-1* cells transformed with YCpHANIP7 grew at 37°C when cultured in SCgal but not when cultured in SCglu (data not shown).

NIP7$^+$ encodes a 181-amino-acid protein with a predicted molecular mass of 20,381 Da and a calculated isoelectric point of 9.28. Recombinant Nip7p migrated as a 22- to 23-kDa protein in SDS-PAGE (not shown). Rabbit polyclonal antiserum raised against recombinant Nip7p recognized a polypeptide in yeast whole-cell extracts with an electrophoretic mobility identical to that of the recombinant protein (see Fig. 7).

A BLAST search of protein sequence databases did not identify any Nip7p homologs. However, a search of expressed-sequence tags identified ORFs with high similarity at the amino acid level in humans, *Caenorhabditis elegans*, and *Arabidopsis thaliana* (Fig. 3). Yeast and human Nip7p proteins are 52.5% identical and 68.75% similar. This high degree of sequence conservation indicates that Nip7p function is evolutionarily conserved among eukaryotes. A search for consensus sequences failed to identify any motifs which might suggest a possible function for Nip7p. Two independent PCR-generated clones of the ts *nip7-1* allele were sequenced and revealed a G-to-A transition at nucleotide 212, resulting in the substitution of aspartic acid for the conserved glycine at position 71 (Fig. 3).

Gene disruption analysis and construction of a conditional lethal mutation of *NIP7*. A null allele of *NIP7* was constructed by removing a 111-bp internal fragment of the *NIP7* ORF and replacing it with the *HIS3* gene (Fig. 1). The resulting *nip7::HIS3* fusion was used to transform a haploid wild-type strain carrying a functional copy of *NIP7* on a *URA3* plasmid (YCpHANIP7). Clones with stable *HIS3* and *URA3* markers were screened for galactose-dependent growth, since the *NIP7* gene on the YCpHANIP7 plasmid is under the control of the *GAL1* promoter (Fig. 1). Nine of 45 Ura$^+$ His$^+$ transformants grew only on galactose-containing medium. None of these nine colonies grew on medium containing 1 mg of 5-fluoro-orotic acid per ml (52), indicating that their growth was dependent on YCpHANIP7. One of these strains, DG438, was selected and crossed to W303-1a. The resulting diploid strain, DG443, lost the *URA3* marker when grown on nonselective medium and was able to grow on 5-fluoro-orotic acid plates, but it retained the *HIS3* marker. The insertion of the *nip7::HIS3* disruption into the genome was confirmed by PCR analysis (data not

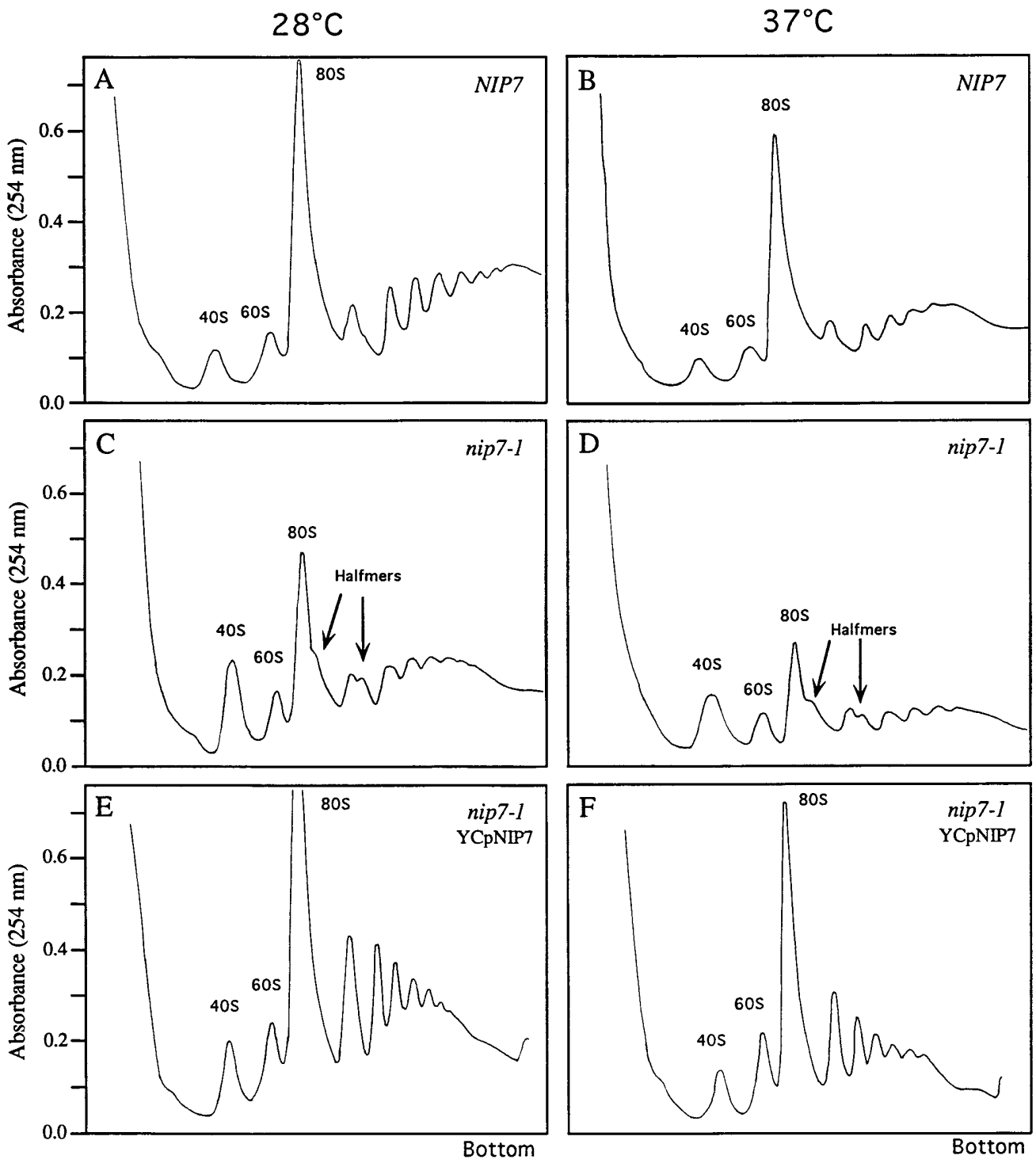

FIG. 2. *nip7-1* cells accumulate halfmer polysomes. Polysomes from strains DG115 (*NIP7*$^+$) (A and B), DG130 (*nip7-1*) (C and D), and DG130 (*nip7-1*) carrying CEN plasmid YCpNIP7, which contains a copy of the wild type *NIP7* gene (E and F), were analyzed. Extracts were prepared from cells grown at 28°C (A, C, and E) or shifted to 37°C for 4 h (B, D, and F). Polysomes were sedimented through 15 to 50% linear sucrose gradients as described in Materials and Methods.

shown). DG443 was sporulated for tetrad analysis. Thirty of 32 tetrads produced by sporulating DG443 yielded two viable spores, and two tetrads produced only one viable spore (data not shown). The viable spores were His$^-$. We conclude that *NIP7* is an essential single-copy gene, which is consistent with the presence of only one copy of this gene in the yeast genome sequence.

The gene disruption analysis described above was performed with a haploid strain that was maintained by a plasmid encoding a copy of *NIP7* (YCpHANIP7) so that derivatives from this

```
    1                                                    50
At  ----------------------------------YCFRLQKKRVYYDSEA
Ce  MRPLTEEETSLVFAKLASFIGDNVSMLIDRNDGDYCFRNHKERVYYCSEN
Hu  MRPLTEEETRVMFEKIAKYIGENLQLLVDRPDGTYCFRLHNDRVYYVSEK
Sc  MRQLTEEETKVVFEKLAGYIGRNISFLVDNKELPHVFRLQKDRVYYVPDH
    ** ****** . * *.* .** *.  *.*  .    ** .  ****  .

    51                                                   100
At  LVKRHTNISRKNLVSCGTCIGIYTHGGSFHLTIMSLNISAANAKNKVWLK
Ce  LMRQAACIAREPLLSFGTCLGKFTKSKKFHLQITALDYLAPYAKFKVWLK
Hu  IMKLAANISGDKLVSLGTCFGKFTKTHKFRLHVTALDYLAPYAKYKVWIK
Sc  VAKLATSVARPNLMSLGICLGKFTKTGKFRLHITSLTVLAKHAKYKIWIK
    . .  . ..   *.* * * * .*.   *.* . .*   *  ** *.*.*
                          ↑
    101                                                  150
At  PTSEMSFLYGNHVLKGGLGRITDSIVPGDGVVVFSMSDVPLGFGIAAKST
Ce  PNAEQQFLYGNNILKSGIARMTDGTPTHAGIVVYSMTDVPLGFGVSAKGT
Hu  PGAEQSFLYGNHVLKSGLGRITENTSQYQGVVVYSMADIPXGFWGCSKST
Sc  PNGEMPFLYGNHVLKAHVGKMSDDIPEHAGVIVFAMNDVPLGFGVSAKST
    *  *  *****..**  ......      *..*..* *.* **  ..*.*

    151                          181
At  QDCRKLDPNGIVVLHQADIGEYLRGEDDL--
Ce  SDSKRADPTALVVLHQCDLGEYLRNESHLA-
Hu  QDLQKSRPHG--------------------
Sc  SESRNMQPTGIVAFRQADIGEYLRDEDTLFT
     . .   * ..*  .* *.***** *  *
```

FIG. 3. Alignment of *S. cerevisiae* Nip7p amino acid sequence with expressed-sequence tags. At, *A. thaliana*; Ce, *C. elegans*; Hu, human; Sc, *S. cerevisiae*. The *A. thaliana* and human sequences lack, respectively, N- and C-terminal sequences. Asterisks indicate identity; periods indicate conserved substitutions. An arrow indicates the conserved glycine 71, which is replaced by aspartic acid in the ts *nip7-1* allele. The sequences were aligned by using Pileup (Genetics Computer Group package).

strain could be generated by substituting other *NIP7*-containing plasmids by plasmid shuffling. DG440 was generated by transforming DG439 (*nip7::HIS3 GAL::*HA-*NIP7*) (see Materials and Methods) with YCpNIP7, which contains a copy of the *NIP7* gene under the control of its own promoter (Fig. 1). YCpHANIP7 was then eliminated by plasmid shuffling. DG439 (HA-*NIP7*) grew slower in YPgal (doubling time, 190 min) than DG440 (*NIP7*) (doubling time, 165 min), possibly either because the HA tag reduced Nip7p function or because overexpression of HA-Nip7p was deleterious for cell growth. Therefore, YCpGNIP7, which lacks the HA tag, was constructed and used to produce DG441 (Fig. 1). As shown in Fig. 4, DG440 (*NIP7*) and DG441 (*GAL::NIP7*) grew at similar rates in YPgal, but DG441 expressed Nip7p at levels that far exceeded those expressed in DG440. A substantial reduction in the level of Nip7p required a 12-h incubation in YPD (Fig. 4B). To avoid possible secondary effects of a long depletion time, another construction was used to more efficiently deplete Nip7p. We had previously observed that *nip7-1* cell extracts contained less Nip7 protein than wild-type extracts. Thus, we constructed DG442, which carries the *nip7-1* allele under control of the *GAL1* promoter (YCpGnip7-1) but is otherwise isogenic to DG440 and DG441. In YPgal, DG442, DG440, and DG441 grew at comparable rates (Fig. 4A). However, growth of DG442 slowed soon after cells were shifted from YPgal to YPD and ceased after 8 h in YPD (Fig. 4A). Moreover, in DG442, Nip7-1p levels were reduced to barely detectable levels within 4 h in YPD (Fig. 4B).

Depletion of Nip7-1p causes a decrease in protein synthesis rates and in 60S ribosome levels. Because *nip7-1* cells are hypersensitive to paromomycin and accumulate halfmer polysomes, we hypothesized that Nip7p probably functions in some aspect of protein synthesis or ribosome biogenesis. Protein synthesis rates were measured by quantifying [^{35}S]methionine incorporation after shifting DG440 (*NIP7*) and DG442 (*GAL1::nip7-1*) to SCglu. As shown in Fig. 5, protein synthesis

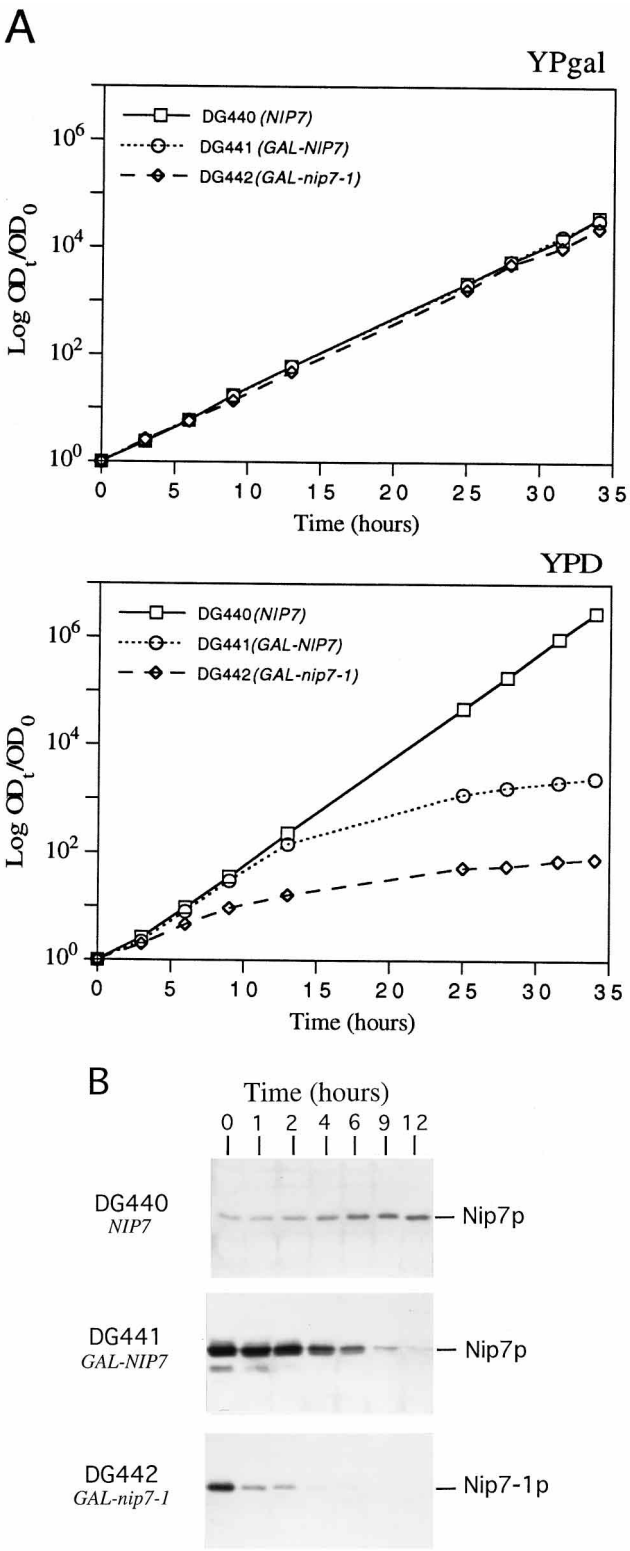

FIG. 4. Nip7-1p depletion causes growth arrest. (A) Growth curves of strains DG440 (*NIP7*), DG441 (*GAL::NIP7*), and DG442 (*GAL1::nip7-1*) grown on YPgal and shifted to YPD at 30°C. OD_{600} values are plotted as log OD_t/OD_0 where t is time in hours after shifting the medium. (B) Immunoblot analysis of Nip7p and Nip7-1p depletion time courses in YPD. Each lane contains total protein isolated from equivalent amounts of cells.

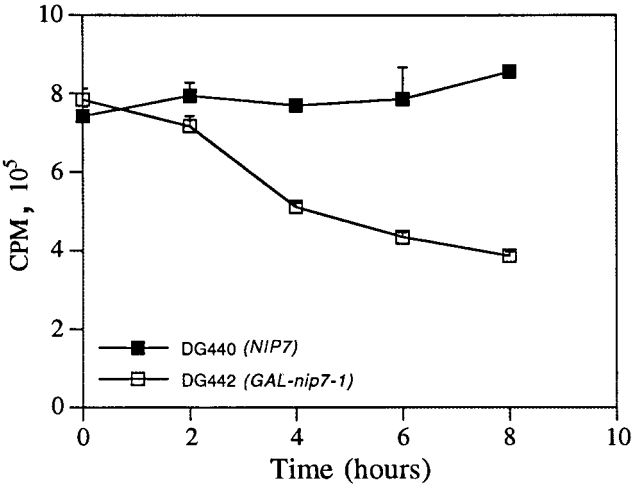

FIG. 5. Protein synthesis rates decline in Nip7-1p-depleted cells. Strains DG440 (*NIP7*) and DG442 (*GAL1::nip7-1*) were grown in SCgal lacking methionine to mid-exponential phase and then shifted to SCglu lacking methionine plus [^{35}S]methionine. Protein synthesis rates were determined as described in Materials and Methods.

rates following the shift to SCglu remained relatively constant in DG440 but decreased significantly in DG442.

Polysome profiles of DG440 (*NIP7*) and DG442 (*GAL1::nip7-1*) were analyzed by using cells maintained in YPgal or shifted to YPD for 5 h. DG440 showed normal polysome profiles in both YPD and YPgal (Fig. 6A). In YPgal, DG442 polysome profiles contained a higher proportion of 80S monosomes relative to polysomes when compared to DG440 polysome profiles, and the free 60S peak appeared to be slightly abnormal (Fig. 6A). This indicated that complementation of the *nip7::HIS3* disruption by *nip7-1* was not complete even though DG442 and DG440 grew at similar rates in YPgal. After depletion of Nip7-1p for 5 h in YPD, DG442 showed a reduction in the amount of polysomes, 80S monosomes, and free 60S subunits and also accumulated halfmer polysomes (compare Fig. 2 and 6A). The reduction in the amount of free 60S subunits indicated an imbalance in the ratio of 40S to 60S subunits, which led us to analyze the amount of 60S subunits in DG442 cells depleted of Nip7-1p for 5 h. In these cells, the level of 60S subunits was reduced by about one-third relative to 60S subunit levels in DG442 growing in YPgal or in DG440 shifted to YPD for 5 h (Fig. 6B). These results suggest that the accumulation of halfmer polysomes was probably due to the decrease in the 60S/40S ratio.

A fraction of Nip7p cosediments with free 60S ribosomal subunits in a salt-sensitive fashion. In the previous section it was shown that depletion of Nip7p led to a decrease in 60S subunit levels. Often, the depletion of individual rproteins leads to a coordinated reduction in the levels of other rproteins that are associated with the same subunit, resulting in an imbalance between 40S and 60S subunits (8, 32, 33, 44). This notion led us to investigate whether Nip7p is a normal component of cytoplasmic 60S subunits. Cell extracts were isolated from W303-1a and fractionated over 15 to 35% linear sucrose gradients (Fig. 7A). The protein compositions of gradient fractions were analyzed by immunoblotting. Tcm1p, which is rprotein L3, was used as a marker for the sedimentation of 60S rproteins. Tcm1p was found within the regions of the gradient containing 60S subunits, 80S monosomes, and polysomal ribosomes but was absent from fractions containing free 40S subunits (Fig. 7B). By contrast, the bulk of Nip7p cosedimented with free 60S subunits, although a moderate amount of Nip7p sedimented near the top of the gradient (Fig. 7B). Fractions containing the 60S peak and the 80S peak were pooled and resedimented. As shown in Fig. 7C, Nip7p cosedimented with 60S subunits but was absent from fractions containing 80S ribosomes. This result indicates that Nip7p is associated with 60S ribosomes but must dissociate before or upon 40S-60S subunit joining and is not, therefore, a permanent component of 60S subunits. The effect of increasing KCl concentrations on the 60S-Nip7p complex was investigated (Fig. 8). In gradients containing 10 mM KCl, equivalent amounts of Nip7p appeared in fractions 2 to 6, which contained non-ribosome-associated proteins, and in fractions 9 to 12, which contained free 60S subunits. A fraction of Nip7p was released from free 60S subunits in 100 mM KCl, and most of the protein was found in the lighter fractions (fractions 2 to 6) in 250 and 500 mM KCl.

Pre-rRNA processing is defective in cells depleted of Nip7-1p. Because Nip7p is not an rprotein and it is therefore unlikely that the deficiency of 60S subunits in *nip7-1* cells is due to the underexpression of rproteins, we investigated the possibility that Nip7p may play a direct role in 60S subunit biogenesis. Since pre-rRNA processing and ribosomal subunit assembly are concerted reactions, the study of pre-rRNA processing by using metabolic labeling and Northern blot analysis has been a powerful approach to detect defects in ribosome biogenesis (16, 55, 56, 58, 59). The pre-rRNA processing pathway in yeast is shown in Fig. 9. For metabolic labeling, cultures of DG440 (*NIP7*) and DG442 (*GAL::nip7-1*) were shifted from SCgal to SCglu and pulse-chase labeled with either [^{3}H]uracil or [*methyl*-^{3}H]methionine. Since the pool of *S*-adenosylmethionine is rapidly saturated and quickly chased (64), shorter periods of labeling and chase times were used in experiments with [*methyl*-^{3}H]methionine.

Both pulse-chase labeling experiments showed similar results. In DG440, 35S pre-rRNA and the 27S and 20S precursors were rapidly chased, indicating a rapid conversion of precursors to mature rRNA, as expected (Fig. 10). In contrast, Nip7-1p-depleted DG442 cells accumulated 35S pre-rRNA and 27S pre-rRNA (most probably 27SB) and were deficient in both 25S rRNA and 18S rRNA (Fig. 10A). The greater deficiency of 25S rRNA relative to 18S rRNA, which was more clearly noted in the [*methyl*-^{3}H]methionine labeling, can be attributed to the accumulation of 27S pre-rRNA (Fig. 10A). Cells depleted of Nip7-1p also accumulated a weakly labeled 23S pre-rRNA. This unusual pre-rRNA was more evident with [*methyl*-^{3}H]methionine labeling. With [^{3}H]uracil, this band was probably masked by the background produced by labeled mRNAs and nascent transcripts. The levels of [*methyl*-^{3}H]methionine labeling are similar in control and Nip7-1p-depleted cells and thus do not indicate a direct role for Nip7p in pre-rRNA methylation.

An analysis of low-molecular-weight rRNAs from the [^{3}H]uracil labeling experiment revealed that 5.8S$_S$ and 5.8S$_L$ rRNA synthesis was reduced in Nip7p-depleted cells (Fig. 10B). As in the case of lower 25S rRNA synthesis, the kinetic delay in 5.8S$_S$ and 5.8S$_L$ rRNA formation was probably due to slow 27S pre-rRNA processing. No alteration in the ratio of 5.8S$_S$ to 5.8S$_L$ rRNAs was detected. The synthesis of 5S rRNA and tRNA was not significantly affected, although DG442 depleted of Nip7-1p showed a lower overall incorporation of [^{3}H]uracil than DG440 (Fig. 10B).

The steady-state levels of pre-rRNAs were determined by hybridization with oligonucleotide probes complementary to 5′ ETS, ITS1, ITS2, and 5.8S rRNA of the 35S pre-rRNA (Fig. 9). RNA was purified from DG440 (*NIP7*) and DG442 (*GAL::nip7-1*) incubated in YPgal or shifted to YPD for

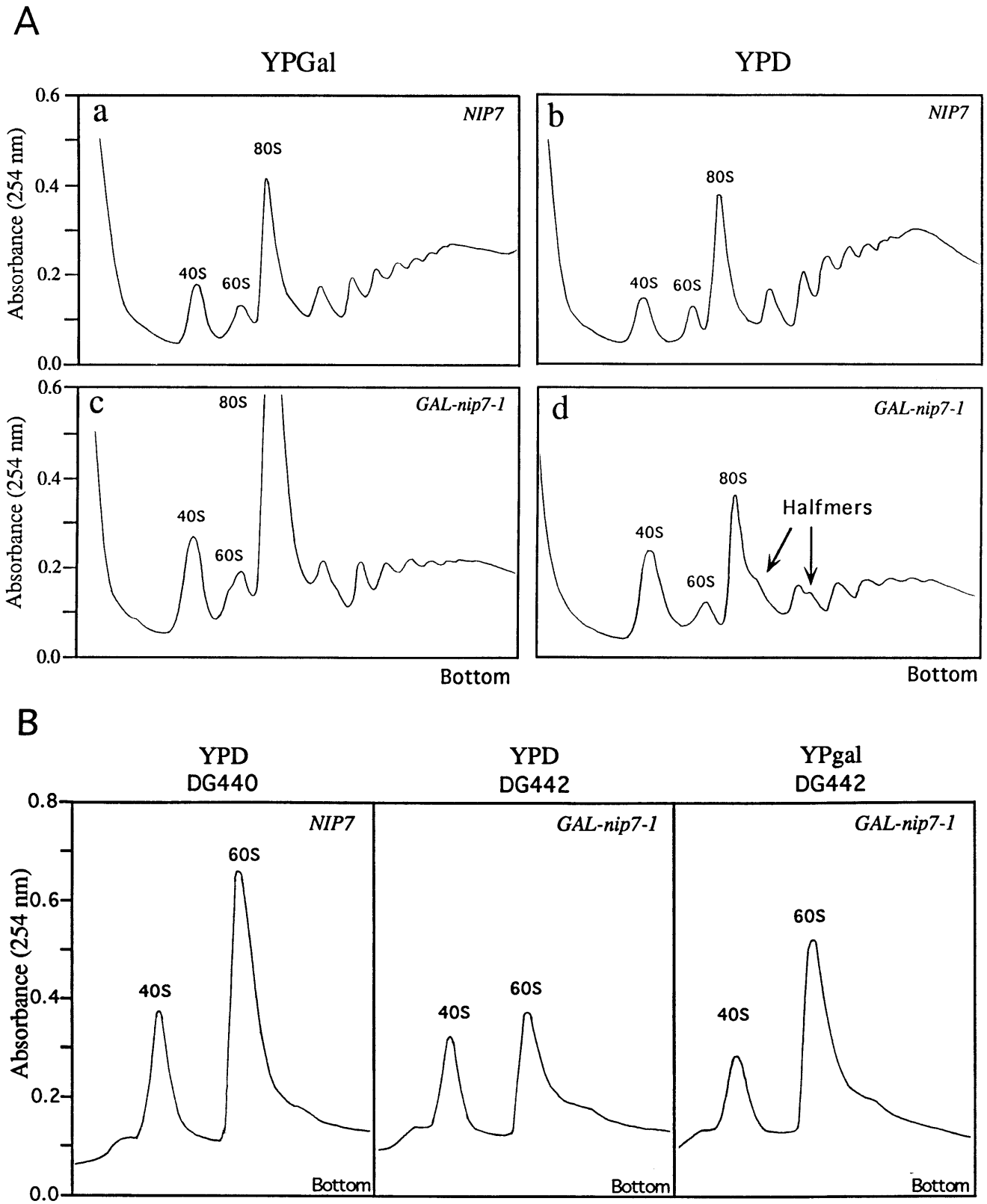

FIG. 6. Nip7-1p depletion results in halfmer accumulation and a decrease in 60S subunit levels. (A) Polysome profiles from strains DG440 (*NIP7*) (a and b) and DG442 (*GAL1::nip7-1*) (c and d) were analyzed. Cultures were grown to mid-exponential phase in YPgal, and then portions were either maintained in YPgal for 5 h (a and c) or switched to YPD for 5 h (b and d). Polysomes were sedimented through 15 to 50% sucrose gradients. (B) Total ribosomes were isolated from strains DG440 (*NIP7*) and DG442 (*GAL::nip7-1*) after 5 h of growth in either YPD or YPgal as described above. Ribosomes were dissociated into 40S and 60S subunits and sedimented through 15 to 35% sucrose gradients as described in Materials and Methods.

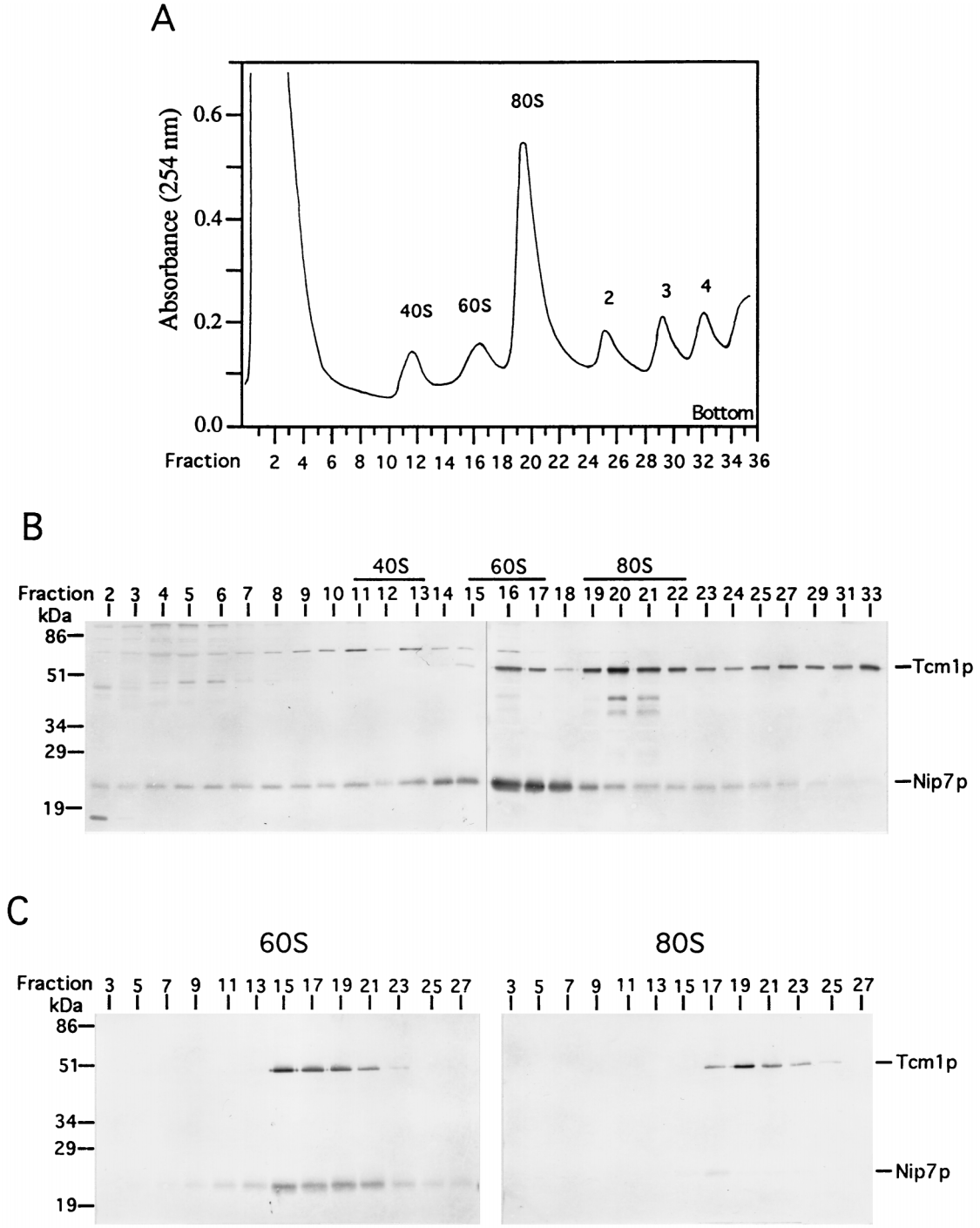

FIG. 7. Nip7p cosediments with free 60S ribosomal subunits. (A) Polysome profile of ribosomes isolated from W303-1a and separated by using a 15 to 35% sucrose gradient. (B) Fractions from the gradient shown in panel A were collected, and proteins were precipitated with 10% TCA and analyzed by SDS-PAGE and immunoblotting. Fractions containing 40S and 60S subunits and 80S monosomes are indicated. (C) 60S- and 80S-containing fractions from a 15 to 35% gradient were pooled, resedimented through 15 to 35% sucrose gradients, and analyzed by immunoblotting. Tcm1p was used as a marker for 60S subunit sedimentation.

various times. Ethidium bromide staining of total RNA revealed a significant decline in the amounts of both 25S and 18S rRNAs upon depletion of Nip7-1p (not shown). As shown in Fig. 11, all of the probes used in the Northern analysis detected large amounts of 35S pre-rRNA in DG442 depleted of Nip7-1p, whereas this pre-rRNA was hardly detectable in DG442 incubated in YPgal or in the control strain (DG440). Northern analysis confirmed the presence of the unusual 23S pre-rRNA in Nip7-1p-depleted cells (Fig. 10A). 23S pre-rRNA was either not visible or barely visible in DG440 or in DG442 expressing Nip7-1p. This 23S pre-rRNA probably spans from the 5′ end of the 5′ ETS to cleavage site A_3, since it was detected by probes

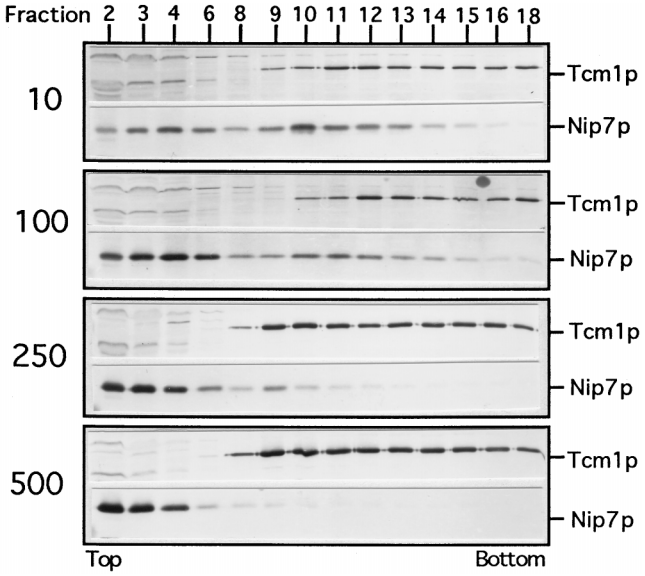

FIG. 8. Effect of salt on Nip7p cosedimentation with 60S ribosomal subunits. W303-1a cells were lysed and sedimented through 15 to 50% sucrose gradients containing either 10, 100, 250, or 500 mM KCl. Fractions were collected, precipitated with 10% TCA, and analyzed by SDS-PAGE and immunoblotting. Tcm1p was used as a marker for 60S subunit sedimentation. Only the regions of the immunoblot containing Nip7p and Tcm1p are shown.

A (upstream A_0), B (upstream A_2), and C (downstream A_2) but was not detected by probe D (in 5.8S) (Fig. 11A to D). Also, a band of approximately 21S was detected by probe A in Nip7p-depleted cells (Fig. 11A). This unusual pre-rRNA probably extends from the 5′ ETS to the 18S rRNA 3′ end. In normal cells, 35S pre-rRNA is rapidly converted to 32S pre-rRNA after processing at A_0 and cleavage at A_1. The accumulation of the 35S pre-rRNA and presence of the unusual 23S pre-rRNA in Nip7-1p-depleted cells indicate that processing at these sites was defective. Finally, probe B, complementary to the region downstream of the 18S rRNA 3′ end and upstream site A_2, revealed a decline in the level of 20S pre-rRNA (Fig. 11B), which was probably due to defects in the processing of 35S pre-rRNA and the unusual 23S pre-rRNA.

Levels of $27SA_2$ pre-rRNA did not increase upon Nip7-1p depletion (Fig. 11C). However, a significant increase in levels of other 27S pre-rRNAs was detected with the three probes complementary to the region comprising both the 5.8S rRNA (probe D) and ITS2 (probes E and F) (Fig. 11D, E, and F). These results suggest that the processing defect in Nip7-1p-depleted cells occurs after $27SA_2$ pre-rRNA is converted to $27SA_3$ or 27SB. Increased levels of these pre-rRNAs are consistent with results obtained with pulse-chase labeling experiments showing accumulation of a 27S pre-rRNA and reduced synthesis of 25S rRNA and 5.8S rRNA. No aberrant precursors containing 5.8S rRNAs were detected. In addition, both in vivo labeling (Fig. 10B) and ethidium bromide staining (not shown) showed that the ratio of $5.8S_S$ to $5.8S_L$ was not affected by Nip7-1p depletion. In conclusion, Northern blot analysis suggests that pathways leading both to 25S and 18S formation are affected by Nip7-1p depletion.

Nip7p localizes to both the cytoplasm and the nucleus. Considering the biochemical evidence that Nip7p is required for pre-rRNA processing, one would predict that Nip7p should function in the nucleolus and not in the cytoplasm as suggested by its cosedimentation with 60S subunits (see above). Therefore, the localization of Nip7p was determined by three methods. As determined by indirect immunofluorescence with a rabbit polyclonal antiserum, Nip7p was distributed evenly in the cytoplasm and nucleus (Fig. 12A). A similar pattern of localization was observed in cells overexpressing Nip7p (Fig. 12E) or Nip7-1p (Fig. 12G). In control experiments, cells incubated with preimmune serum (Fig. 12C) or cells depleted of Nip7-1p incubated with immune serum (Fig. 12I) showed only background fluorescence. These results indicate that Nip7p is at least partly localized in the cytoplasm, which is consistent with the cosedimentation of Nip7p with 60S subunits. Cell fractionation analysis indicated that the bulk of Nip7p was associated with nuclear fractions (Fig. 13). Fractions were also probed with antibodies directed against the translation initiation factor eIF-2α, the nucleolar protein 1 (Nop1p), and the 60S subunit ribosomal protein 3 (Tcm1p). Nop1p, which was previously localized to the nucleolus (1), was detected mostly in association with nuclear fractions. As expected for a translation factor, eIF-2α was found predominately in cytoplasmic fractions. Unexpectedly, though, a significant amount of Tcm1p was found in nuclear fractions (Fig. 13), suggesting that the nuclear fractions might be contaminated with cytoplasmic proteins. Were Nip7p a cytoplasmic protein, the contamination of nuclear fractions with cytoplasm might lead to the artifactual conclusion that large amounts of Nip7p are nuclear. In order to directly visualize Nip7p subcellular localization, a fusion protein between Nip7p and GFP was constructed. Interestingly, the Nip7p-GFP fusion protein produced an intense crescent-shaped fluorescence signal that is consistent with nucleolar localization (Fig. 14). Less-intense fluorescence was observed in the cytoplasm. Unfortunately, despite the fact that the lo-

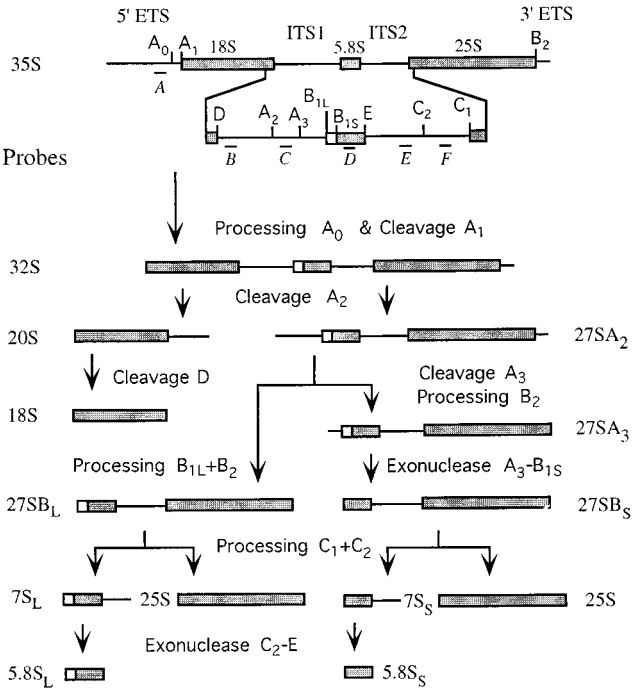

FIG. 9. Organization and major processing pathways of yeast pre-rRNA. The 35S pre-rRNA comprises the sequences of the mature 18S, 5.8S, and 25S rRNAs flanked by the internal transcribed spacers ITS1 and ITS2 and by external transcribed spacers at the 5′ end (5′ ETS) and at the 3′ end (3′ ETS). Cleavage sites, major steps involving endonucleolytic and exonucleolytic processing, and major pre-rRNA intermediates are indicated. The relative positions of the oligonucleotides (probes) used in Northern analysis are also indicated.

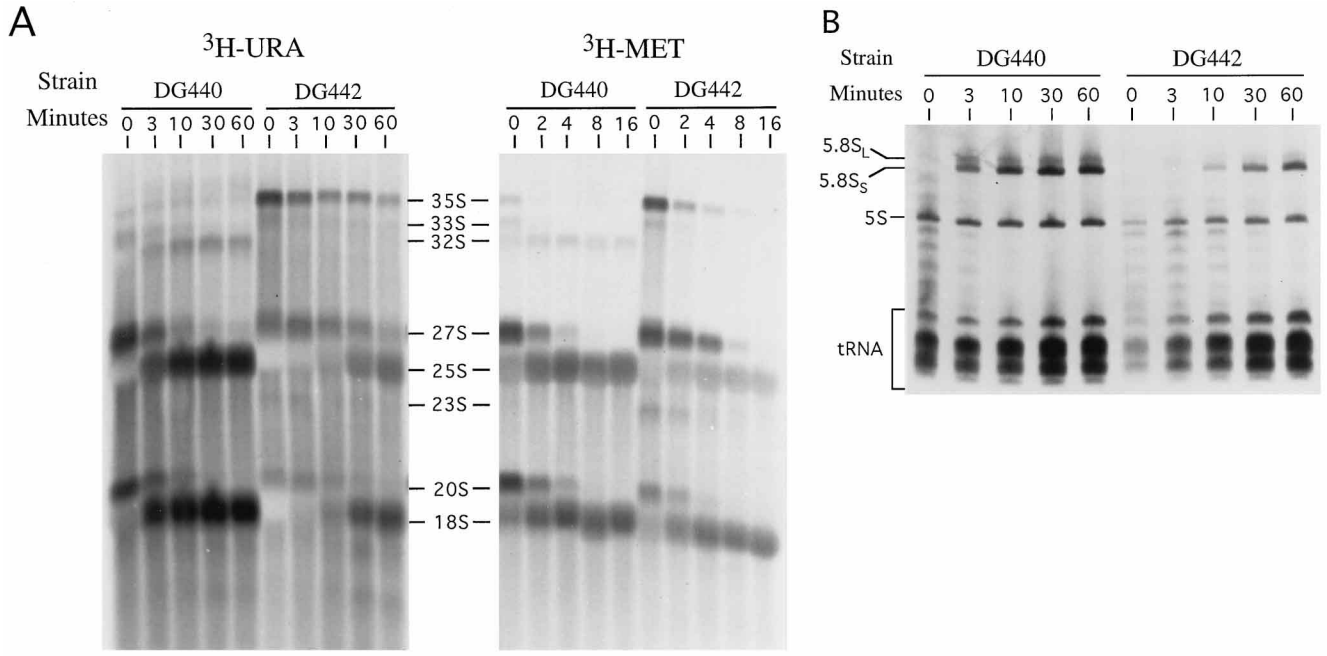

FIG. 10. Pulse-chase labeling analysis of pre-rRNAs in cells depleted of Nip7-1p. Processing of rRNA precursors in strains DG440 (*NIP7*) and DG442 (*GAL1::nip7-1*) shifted from SCgal to SCglu for 4 h was assayed. After the 4 h, cultures were divided into two fractions for pulse-chase labeling. Cultures were pulse-labeled with either [^{3}H]uracil or [*methyl*-^{3}H]methionine and chased with an excess of unlabeled uracil or methionine, respectively, for the indicated times. RNA samples were extracted and analyzed as described in Materials and Methods. (A) Analysis of high-molecular-weight rRNAs labeled with [^{3}H]uracil (^{3}H-URA) or [*methyl*-^{3}H]methionine (^{3}H-MET). (B) Analysis of low-molecular-weight rRNAs labeled with [^{3}H]uracil. The same amount of total RNA (8 μg) was loaded in each lane. The positions of major pre-rRNAs and rRNAs are indicated.

calization of the fusion protein was consistent with the demonstrated role for Nip7p in nucleolar pre-rRNA processing, the Nip7p-GFP fusion protein did not complement the *nip7::HIS3* disruption. In summary, cell fractionation and GFP fluorescence suggest that a substantial amount of Nip7p is present inside the nucleus, possibly in the nucleolus, but indirect immunofluorescence and cosedimentation analysis suggest that a fraction of Nip7p is located in the cytoplasm in association with free 60S subunits.

DISCUSSION

NIP7 encodes an essential 21-kDa protein that is conserved among eukaryotes (Fig. 3). To assess the effect of depleting Nip7p in yeast, the ts allele *nip7-1* was placed on a plasmid under the control of the *GAL1* promoter in a *NIP7*Δ strain. Depletion of Nip7-1p resulted in decreased protein synthesis rates, reduced 60S subunit levels, accumulation of halfmer polysomes, and defects in pre-rRNA processing. Decreased protein synthesis rates and accumulation of halfmer polysomes were most probably due to the reduction in 60S subunit levels. Reductions in 60S subunit levels have previously been reported for depletion or mutation of several 60S subunit rproteins, such as L1, L16, and L46 (8, 32, 33, 44). Nip7p, however, does not behave as a permanent component of the 60S subunit, because it was found in association with free 60S subunits but not with 80S monosomes or with polysomes. In addition, Nip7p was released from 60S subunits by relatively low salt concentrations (100 to 250 mM KCl) (Fig. 8) that are typically insufficient to dissociate bona fide rproteins (41). The protocol employed in these experiments was developed for the analysis of cytoplasmic ribosomal subunits and polysomes. Although there may be some leakage from the nucleus during cell extract preparation, which we cannot rule out, it is likely that the Nip7p-containing 60S subunits were cytoplasmic.

Association of Nip7p with free cytoplasmic 60S subunits is most consistent with the results obtained by indirect immunofluorescence, which provided the strongest evidence for the presence of Nip7p in the cytoplasm of fixed cells. The mostly nuclear localization of a Nip7p-GFP fusion protein in living cells can be explained if we postulate that nucleolar Nip7p is inaccessible to anti-Nip7p antibodies. Together, the localization data are consistent with the model that Nip7p is exported from the nucleus in association with 60S subunits and is released from 60S subunits upon or after binding to the 40S subunit. Possibly, Nip7 participates in some aspect of 60S subunit assembly in the cytoplasm, which is consistent with data reported by Tollervey et al. (59) showing that 60S subunits undergo late assembling steps in the cytoplasm. On the other hand, the presence of Nip7p in the nucleolus, as indicated by the localization of the Nip7p-GFP fusion protein, also supports a role for this protein in pre-rRNA processing or ribosome assembly. Although Nip7p does not contain a canonical nuclear localization sequence (NLS), it could either contain an atypical NLS or be imported piggyback fashion in a complex with other NLS-containing proteins.

In Nip7-1p-depleted cells the reduction of 60S subunit levels appeared to be caused by a primary defect in pre-rRNA processing. Pulse-chase labeling showed that synthesis of the 25S and 5.8S rRNAs was kinetically delayed at the level of 27S pre-rRNA processing. This result was confirmed by Northern analysis, which showed an increase in 27S pre-rRNA steady-state levels. The pre-rRNA processing defects observed in Nip7-1p-depleted cells are similar to the defects described for *drs1* cells and for cells depleted of Dbp3p and Nop2p, which were shown to specifically affect 60S subunit biogenesis (16, 42,

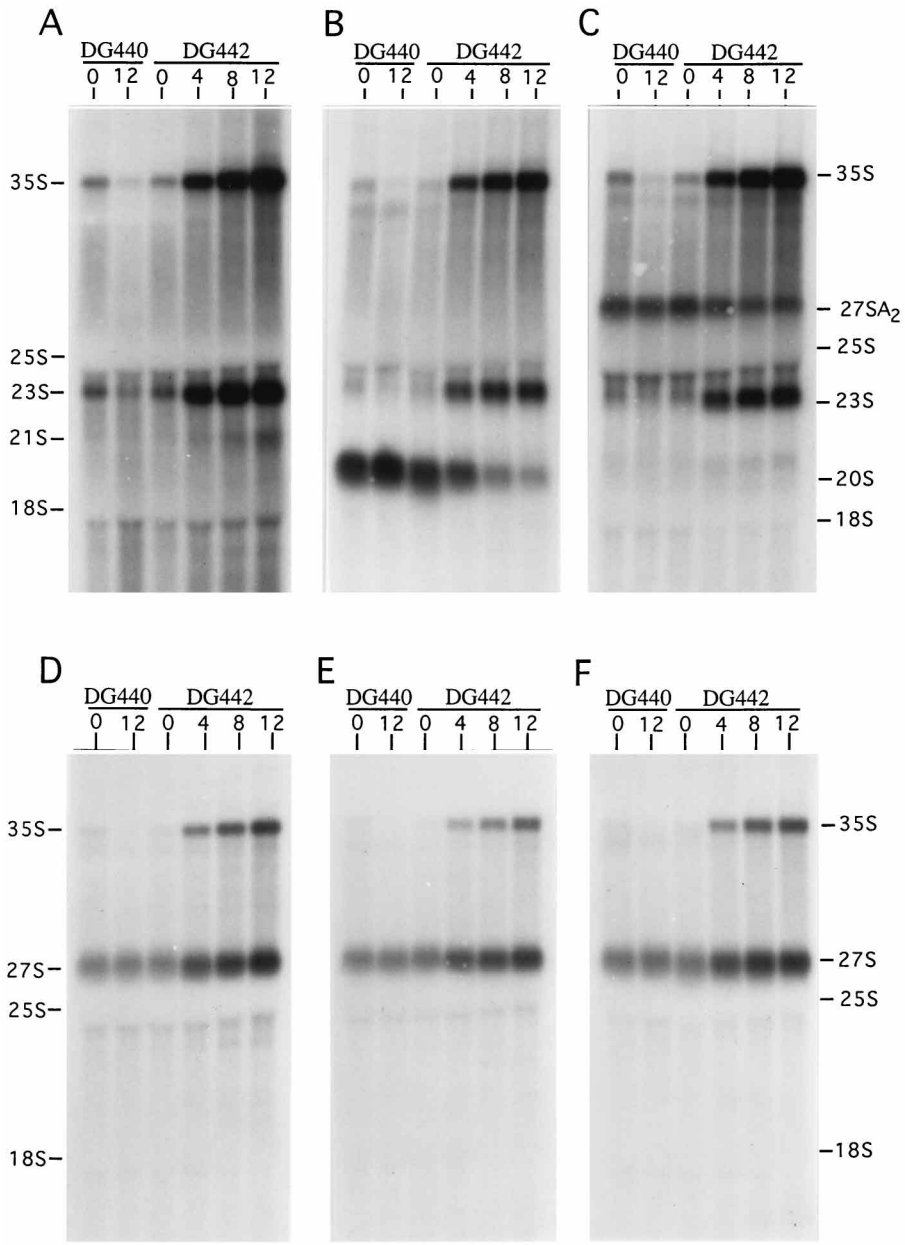

FIG. 11. Effect of Nip7-1p depletion on pre-rRNA steady-state level. RNA was extracted from strain DG440 (*NIP7*) at time zero and 12 h after transfer to YPD and from strain DG442 (*GAL1::nip7-1*) at time zero and 4, 8, and 12 h after transfer to YPD. RNAs were separated on agarose gels and analyzed by Northern hybridization with oligonucleotides complementary to different regions of the 35S pre-RNA (Fig. 9). (A) Probe A, upstream site A_0 in the 5′ ETS; (B) probe B, downstream 18S rRNA 3′ end/upstream site A_2 in ITS1; (C) probe C, between sites A_2 and A_3 in ITS1; (D) probe D, in the 5.8S rRNA; (E) probe E, upstream site C_2 in ITS2; (F) probe F, between sites C_2 and C_1 in ITS2. The positions of the major precursors as well as the 25S and 18S rRNAs are indicated.

65). In these three cases, inhibition of 25S rRNA synthesis and accumulation of 27S pre-rRNA were noted. Cells depleted of Dbp3p, a putative RNA helicase, are defective for processing at site A_3, which results in accumulation of the $27SA_2$ pre-rRNA (65), whereas cells depleted of Nop2p, a protein containing conserved methylase motifs, accumulated 27SB pre-rRNA (16). In Nip7p-depleted cells, the steady-state level of the $27SA_2$ pre-rRNA was not affected, indicating that processing is impaired after the $27SA_2$ pre-rRNA is converted to $27SA_3$ or 27SB pre-rRNA. Both $27SB_S$ and $27SB_L$ pre-rRNA processing seemed to be inhibited to the same extent, since no alteration in the $5.8S_S/5.8S_L$ ratio was observed. Another nucleolar protein whose depletion resulted in accumulation of 27S pre-rRNA is Nop3p/Np13p. However, depletion of this protein also blocked 18S rRNA synthesis (4, 45). Mutation of *SBP4* and depletion of Nop4/Nop77p also impaired 25S rRNA synthesis, but in these cases the pre-rRNA processing defect involved destabilization of the 27S pre-rRNA (3, 46, 55).

Cells depleted of Nip7-1p also accumulated 35S pre-rRNA and an unusual 23S pre-rRNA. The 23S pre-rRNA is formed by direct cleavage of the 35S pre-rRNA at site A_3 when processing at sites A_0, A_1, and A_2 is inhibited, which appears to be part of an alternative pathway to 18S rRNA (45). Although it is not clear whether accumulation of 35S and 23S pre-rRNAs

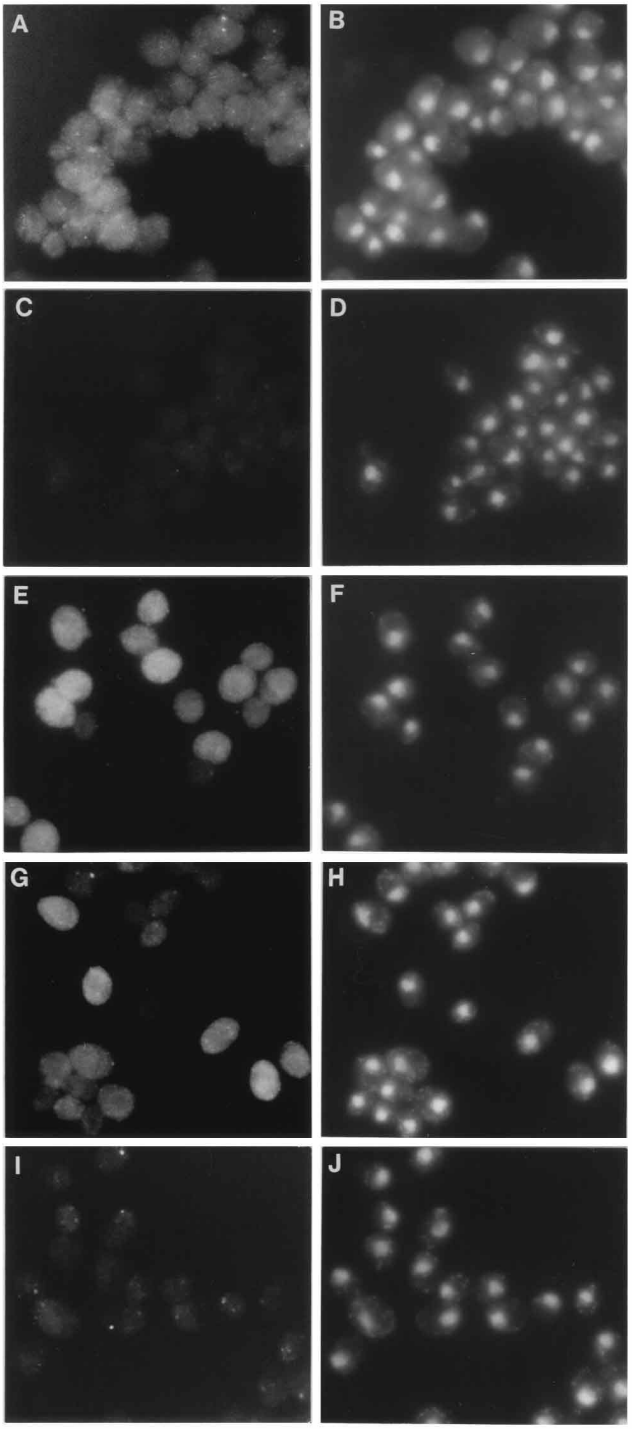

FIG. 12. Indirect immunofluorescence analysis of Nip7p localization. Indirect immunofluorescence was performed with W303-1a incubated with immune serum (A) and preimmune serum (C), with W303-1a carrying plasmid YCpG-NIP7, and overexpressing Nip7p, incubated with immune serum (E), and with DG442 (*GAL1::nip7-1*), overexpressing Nip7-1p (G) or depleted of Nip7-1p in YPD for 4 h (I), incubated with immune serum. Cells were incubated with a 1:3,000 dilution of preimmune serum or antiserum followed by fluorescein-conjugated anti-rabbit IgG. Panels B, D, F, H, and J show the same cells as in panels A, C, E, G, and I, respectively, double stained with DAPI.

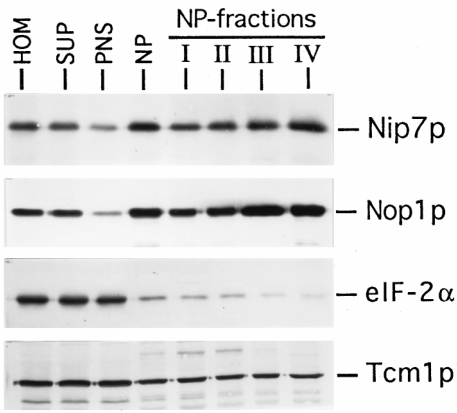

FIG. 13. Analysis of Nip7p distribution in subcellular fraction. W303-1a cells were subfractionated by using sucrose step gradients into eight fractions: total cell homogenate (HOM), supernatant (containing nuclei) without cell debris (which was removed by low-speed centrifugation) (SUP), postnuclear supernatant (PNS), crude nuclear pellet (NP), and four nuclear subfractions produced by further fractionation of the NP on sucrose step gradients (I, soluble proteins; II, mitochondria; III and IV, nuclei). Fractions were probed by immunoblotting with rabbit antibodies directed against Nip7p and eIF-2α and mouse monoclonal antibodies raised against Tcm1p and Nop1p. Equivalent amounts of protein from each fraction was loaded on the gel. The gels used for immunoblot analysis contained the same amount of protein.

was caused by a direct effect of Nip7-1p depletion, these results potentially implicate Nip7p in 18S rRNA synthesis. However, considering that both the steady-state level of 40S subunits and 18S rRNA synthesis were not as drastically affected as the level of 60S subunits and 25S rRNA synthesis in Nip7-1p-depleted cells, we favor the hypothesis that the accumulation of 35S and 23S pre-rRNAs is a consequence of defective 27S pre-rRNA

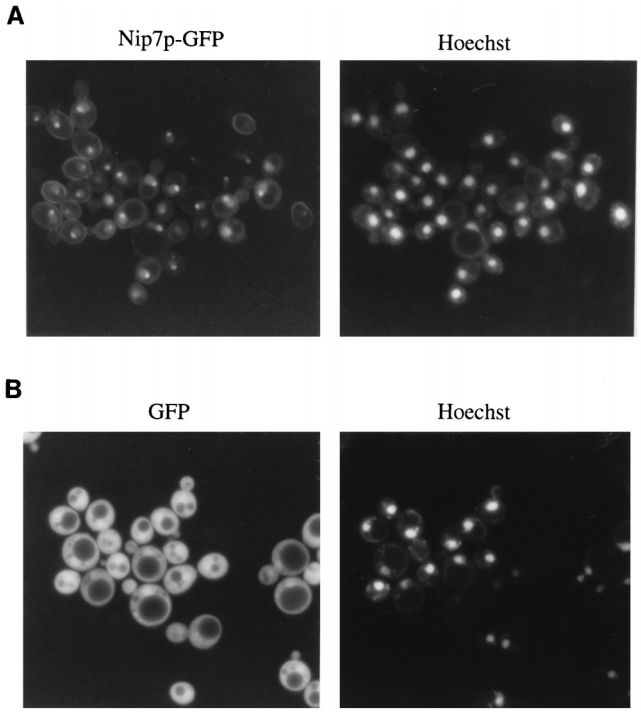

FIG. 14. Localization of Nip7p-GFP. GFP and Hoechst fluorescence of W303-1a cells expressing Nip7p-GFP (A) or GFP (B) is shown.

processing rather than a direct processing defect caused by Nip7-1p depletion. This hypothesis is consistent with the results reported for depletion of Dbp3p, Nop2p, and Nop4p/Nop77p, which have been shown to specifically affect 25S rRNA synthesis (3, 16, 55, 65). Depletion of any of these proteins also resulted in reduced processing of 35S pre-rRNA and presence of the unusual 23S pre-rRNA, which were attributed to a generalized reduction in the processing rate caused by defective 27S pre-rRNA processing (3, 16, 55, 65).

The results obtained with [*methyl*-^{3}H]methionine labeling do not implicate Nip7p in pre-rRNA methylation. The levels of pre-rRNA labeling in control and in Nip7-1p-depleted cells were similar. The reduced level of 25S rRNA in Nip7-1p-depleted cells can be explained by the delay in 25S rRNA synthesis due to defective 27S pre-rRNAs processing. This interpretation is supported by results obtained with [^{3}H]uracil labeling, which also revealed a delay in 27S pre-rRNA processing in Nip7-1p-depleted cells.

NIP7 is a novel gene that is conserved among eukaryotes from yeast to humans. The depletion of Nip7-1p causes a significant defect in pre-rRNA processing which, we argue, leads to the depletion of 60S subunits relative to 40S subunits. The putative localization of a significant fraction of Nip7p-GFP fusion protein to the nucleolus is consistent with this model. However, the localization of some Nip7p in the cytoplasm, where it associates with free 60S subunits, suggests that Nip7p also functions during late 60S maturation stages in the cytoplasm or in either early stages of translation initiation or late stages of termination. Genetic and biochemical studies aimed at identifying Nip7p-associated cellular factors should further elucidate Nip7p function.

ACKNOWLEDGMENTS

We are grateful to John Aris for providing anti-Nop1p antibody, Jonathan Warner for providing anti-Tcm1p antibody, and John McCarthy for providing anti-eIF-2α antibody. We are also grateful to Chris Apolito for excellent technical assistance.

This work was supported by American Cancer Society grant BE-104 (to D.S.G.) and by NIH grant R01GM12702 (to F.S.).

REFERENCES

1. **Aris, J. P., and G. Blobel.** 1988. Identification and characterization of a yeast nucleolar protein that is similar to a rat liver nucleolar protein. J. Cell Biol. **107:**17–31.
2. **Belev, T. N., M. Sigh, and J. E. G. McCarthy.** 1991. A fully modular vector system for the optimization of gene expression in *Escherichia coli*. Plasmid **26:**147–150.
3. **Bergès, T., E. Petfalski, D. Tollervey, and E. C. Hurt.** 1994. Synthetic lethality with fibrillarin identifies NOP77p, a nucleolar protein required for pre-rRNA processing and modification. EMBO J. **13:**3136–3148.
4. **Bossie, M. A., C. DeHoratius, G. Barcelo, and P. Silver.** 1992. A mutant nuclear protein with similarity to RNA binding proteins interferes with nuclear import in yeast. Mol. Biol. Cell. **3:**875–893.
5. **Chamberlain, J. R., E. Pagán-Ramos, D. W. Kindelberger, and D. R. Engelke.** 1996. An RNase P RNA subunit mutation affects ribosomal RNA processing. Nucleic Acids Res. **24:**3158–3166.
6. **Chu, S., R. H. Archer, J. M. Zengel, and L. Lindahl.** 1994. The RNA of RNase MRP is required for normal processing of ribosomal RNA. Proc. Natl. Acad. Sci. USA **91:**659–663.
7. **Davies, J. L., L. Gorini, and B. D. Davies.** 1965. Misreading of RNA codewords induced by aminoglycoside antibiotics. Mol. Pharmacol. **1:**93–106.
8. **Deshmukh, M., Y.-F. Tsay, A. G. Paulovich, and J. L. Woolford, Jr.** 1993. Yeast ribosomal protein L1 is required for the stability of newly synthesized 5S rRNA and the assembly of 60S ribosomal subunits. Mol. Cell. Biol. **13:**2835–2845.
9. **Devereux, J., P. Haeberli, and O. Smithies.** 1984. A comprehensive set of sequence analysis programs for the VAX. Nucleic Acids Res. **12:**387–395.
10. **El-Baradi, T. T. A. L., A. F. M. van der Sande, W. H. Mager, H. A. Raué, and R. J. Planta.** 1886. The cellular level of yeast ribosomal protein L25 is controlled principally by rapid degradation of excess protein. Curr. Genet. **10:**733–739.
11. **Gietz, R. D., and A. Sugino.** 1988. New yeast-*Escherichia coli* shuttle vectors constructed with in vitro mutagenized yeast genes lacking six-base pair restriction sites. Gene **74:**527–534.
12. **Girard, J.-P., H. Lehtonen, M. Caizergues-Ferrer, F. Amalric, D. Tollervey, and B. Lapeyre.** 1992. GAR1 is an essential small nucleolar RNP protein required for pre-rRNA processing in yeast. EMBO J. **11:**673–682.
13. **Gu, Z., R. P. Moerschell, F. Sherman, and D. S. Goldfarb.** 1992. *NIP1*, a gene required for nuclear transport in yeast. Proc. Natl. Acad. Sci. USA **89:**10355–10359.
14. **Helser, T. L., R. A. Baan, and A. E. Dahlberg.** 1981. Characterization of a 40S ribosomal subunit complex in polyribosomes of *Saccharomyces cerevisiae* treated with cycloheximide. Mol. Cell. Biol. **1:**51–57.
15. **Henry, Y., H. Wood, J. P. Morrisey, E. Petfalski, S. Kearsey, and D. Tollervey.** 1994. The 5′ end of yeast 5.8S rRNA is generated by exonucleases from an upstream cleavage site. EMBO J. **13:**2452–2463.
16. **Hong, B., J. S. Brockenbrough, P. Wu, and J. P. Aris.** 1997. Nop2p is required for pre-rRNA processing and 60S ribosome subunit synthesis in yeast. Mol. Cell. Biol. **17:**378–388.
17. **Hughes, J. M. X., and M. Ares, Jr.** 1991. Depletion of U3 small nucleolar RNA inhibits cleavage in the 5′ external transcribed spacer of yeast pre-ribosomal RNA and impairs formation of 18S ribosomal RNA. EMBO J. **10:**4231–4239.
18. **Hurt, E. C., A. McDowall, and T. Schimmang.** 1988. Nucleolar and nuclear envelope proteins of the yeast *Saccharomyces cerevisiae*. Eur. J. Cell. Biol. **46:**554–563.
19. **Jansen, R., D. Tollervey, and E. C. Hurt.** 1993. A U3 snoRNP protein with homology to splicing factor PRP4 and Gβ domains is required for ribosomal RNA processing. EMBO J. **12:**2549–2558.
20. **Köhrer, K., and H. Domdey.** 1991. Preparation of high molecular weight RNA. Methods Enzymol. **194:**398–405.
21. **Kondo, K., and M. Inouye.** 1992. Yeast NSR1 protein that has structural similarity to mammalian nucleolin is involved in pre-rRNA processing. J. Biol. Chem. **267:**16252–16258.
22. **Kondo, K., L. R. Z. Kowalski, and M. Inouye.** 1992. Cold shock induction of yeast NSR1 protein and its role in pre-rRNA processing. J. Biol. Chem. **267:**16259–16265.
23. **Kruiswijk, T., R. J. Planta, and J. M. Krop.** The course of the assembly of ribosomal subunits in yeast. Biochim. Biophys. Acta **517:**378–389.
24. **Laemmli, U. K.** 1970. Cleavage of structural proteins during the assembly of the head of bacteriophage T4. Nature **227:**680–685.
25. **Lafontaine, D., J. Vandenhaute, and D. Tollervey.** 1995. The 18S rRNA dimethylase Dim1p is required for pre-ribosomal RNA processing in yeast. Genes Dev. **9:**2470–2481.
26. **Lee, W.-C., D. Zabetakis, and T. Mélèse.** 1992. *NSR1* is required for pre-rRNA processing and for the proper maintenance of steady-state levels of ribosomal subunits. Mol. Cell. Biol. **12:**3865–3871.
27. **Li, H. V., J. Zagorski, and M. J. Fournier.** 1990. Depletion of U14 small nuclear RNA snR128 disrupts production of 18S rRNA in *Saccharomyces cerevisiae*. Mol. Cell. Biol. **10:**1145–1152.
28. **Liu, H., J. Krizek, and A. Bretscher.** 1992. Construction of a *GAL1*-regulated yeast cDNA expression library and its application to the identification of genes whose overexpression causes lethality in yeast. Genetics **132:**665–673.
29. **Lygerou, Z., P. Mitchell, E. Petfalski, B. Séraphin, and D. Tollervey.** 1994. The *POP1* gene encodes a protein component common to the RNase MRP and RNase P ribonucleoproteins. Genes Dev. **8:**1423–1433.
30. **Maicas, E., F. G. Pluthero, and J. D. Friesen.** 1988. The accumulation of three yeast ribosomal proteins under conditions of excess mRNA is determined primarily by fast protein decay. Mol. Cell. Biol. **8:**169–175.
31. **Mitchell, P., E. Petfalski, and D. Tollervey.** 1996. The 3′ end of yeast 5.8S rRNA is generated by an exonuclease processing mechanism. Genes Dev. **10:**502–513.
32. **Moritz, M., A. G. Paulovich, Y.-F. Tsay, and J. L. Woolford, Jr.** 1990. Depletion of yeast ribosomal proteins L16 and rp59 disrupts ribosome assembly. J. Cell Biol. **111:**2261–2274.
33. **Moritz, M., B. A. Pulaski, and J. L. Woolford, Jr.** 1991. Assembly of 60S ribosomal subunits is perturbed in temperature-sensitive yeast mutants defective in ribosomal protein L16. Mol. Cell. Biol. **11:**5681–5692.
34. **Morrissey, J. P., and D. Tollervey.** 1993. Yeast snR30 is a small nucleolar RNA required for 18S rRNA synthesis. Mol. Cell. Biol. **13:**2469–2477.
35. **Ng, D. T. W., and P. Walter.** 1996. ER membrane protein complex required for nuclear fusion. J. Cell Biol. **132:**499–509.
36. **O'Day, C. L., F. Chavanikamannil, and J. Abelson.** 1996. 18S rRNA processing requires the RNA helicase-like protein Rrp3p. Nucleic Acids Res. **24:**3201–3207.
37. **Palmer, E., J. M. Wilhelm, and F. Sherman.** 1979. Phenotypic suppression of nonsense mutants in yeast by aminoglycoside antibiotics. Nature **277:**148–150.
38. **Planta, R. J., P. M. Gonçalves, and W. H. Mager.** 1996. Global regulators of ribosome biosynthesis in yeast. Biochem. Cell Biol. **73:**825–834.
39. **Pokrywka, N. J., and D. S. Goldfarb.** 1995. Nuclear export pathways of tRNA and 40S ribosomes include both common and specific intermediates. J. Biol. Chem. **270:**3619–3624.
40. **Proweller, A., and S. Butler.** 1994. Efficient translation of poly(A)-deficient

mRNAs in *Saccharomyces cerevisiae*. Genes Dev. **8:**2629–2640.
41. **Raué, H. A., W. H. Mager, and R. J. Planta.** 1991. Structural and functional analysis of yeast ribosomal proteins. Methods Enzymol. **194:**453–477.
42. **Ripmaster, T. L., G. P. Vaughn, and J. L. Woolford, Jr.** 1992. A putative ATP-dependent RNA helicase involved in *Saccharomyces cerevisiae* ribosome assembly. Proc. Natl. Acad. Sci. USA **89:**11131–11135.
43. **Rose, M. D., P. Novick, J. H. Thomas, D. Botstein, and G. R. Fink.** 1987. A *Saccharomyces cerevisiae* genomic plasmid bank based on a centromere-containing shuttle vector. Gene **60:**237–242.
44. **Rotenberg, M. O., M. Moritz, and J. L. Woolford, Jr.** 1988. Depletion of *Saccharomyces cerevisiae* ribosomal protein L16 causes a decrease in 60S ribosomal subunits and formation of half-mer polyribosomes. Genes Dev. **2:**160–172.
45. **Russell, I. D., and D. Tollervey.** 1992. NOP3 is an essential yeast protein which is required for pre-rRNA processing. J. Cell Biol. **119:**737–747.
46. **Sachs, A., and R. W. Davis.** 1990. Translation initiation and ribosomal biogenesis: involvement of a putative rRNA helicase and RPL46. Science **247:**1077–1079.
47. **Sambrook, J., T. Maniatis, and E. F. Fritsch.** 1989. Molecular cloning: a laboratory manual, 2nd ed. Cold Spring Harbor Laboratory Press, Cold Spring Harbor, N.Y.
48. **Schmitt, M. E., and D. A. Clayton.** 1993. Nuclear RNase MRP is required for correct processing of pre-5.8S rRNA in *Saccharomyces cerevisiae*. Mol. Cell. Biol. **13:**7935–7941.
49. **Schneppe, B., W. Eichner, and J. E. G. McCarthy.** 1994. Translation regulation of a recombinant operon containing human platelet-derived growth factor (PGDF)-encoding genes in *Escherichia coli*: genetic titration of the peptide chains of the heterodimer AB. Gene **143:**201–209.
50. **Sherman, F., G. R. Fink, and J. B. Hicks.** 1986. Laboratory course manual for methods in yeast genetics. Cold Spring Harbor Laboratory Press, Cold Spring Harbor, N.Y.
51. **Sherman, F.** 1991. Getting started with yeast. Methods Enzymol. **194:**3–21.
52. **Sikorski, R. S., and J. D. Boeke.** 1991. *In vitro* mutagenesis and plasmid shuffling: from cloned gene to mutant yeast. Methods Enzymol. **194:**302–318.
53. **Singh, A., D. Ursic, and J. Davies.** 1979. Phenotypic suppression and misreading in *Saccharomyces cerevisiae*. Nature **277:**146–148.
54. **Stevens, A., C. L. Hsu, K. R. Isham, and F. W. Larimer.** 1991. Fragments of the internal transcribed spacer 1 of pre-rRNA accumulate in *Saccharomyces cerevisiae* lacking 5′-3′ exoribonuclease 1. J. Bacteriol. **173:**7024–7028.
55. **Sun, C., and J. L. Woolford, Jr.** 1994. The yeast *NOP4* gene product is an essential nucleolar protein required for pre-rRNA processing and accumulation of 60S ribosomal subunits. EMBO J. **13:**3127–3135.
56. **Tollervey, D.** 1987. A yeast small nuclear RNA is required for normal processing of pre-ribosomal RNA. EMBO J. **6:**4169–4175.
57. **Tollervey, D.** 1996. Trans-acting factors in ribosome synthesis. Exp. Cell Res. **229:**226–232.
58. **Tollervey, D., H. Lehtonen, M. Carmo-Fonseca, and E. C. Hurt.** 1991. The small nucleolar RNP protein Nop1 (fibrillarin) is required for pre-rRNA processing in yeast. EMBO J. **10:**573–583.
59. **Tollervey, D., H. Lehtonen, R. Jansen, H. Kern, and E. C. Hurt.** 1993. Temperature-sensitive mutations demonstrate roles for yeast fibrillarin in pre-rRNA processing, pre-RNA methylation, and ribosome assembly. Cell **72:**443–457.
60. **Towbin, H., T. Staehelin, and J. Gordon.** 1979. Electrophoretic transfer of proteins from polyacrylamide gels to nitrocellulose sheets: procedure and some applications. Proc. Natl. Acad. Sci. USA **76:**4350–4354.
61. **Tsay, Y.-F., J. R. Thompson, M. O. Rotenberg, J. C. Larkin, and J. L. Woolford, Jr.** 1988. Ribosomal protein synthesis is not regulated at the translational level in *Saccharomyces cerevisiae*: balanced accumulation of ribosomal proteins L16 and rp59 is mediated by turnover of excess protein. Genes Dev. **2:**664–676.
62. **Udem, S. A., and J. R. Warner.** 1973. The cytoplasmic maturation of a ribosomal precursor ribonucleic acid in yeast. J. Biol. Chem. **248:**1412–1416.
63. **Venema, J., and D. Tollervey.** 1996. RRP5 is required for formation of both 18S and 5.8S rRNA in yeast. EMBO J. **15:**5701–5714.
64. **Warner, J. R.** 1991. Labeling of RNA and phosphoproteins in *Saccharomyces cerevisiae*. Methods Enzymol. **194:**423–428.
65. **Weaver, P. L., C. Sun, and T.-H. Chang.** 1997. Dbp3p, a putative RNA helicase in *Saccharomyces cerevisiae*, is required for efficient pre-rRNA processing predominantly at site A_3. Mol. Cell. Biol. **17:**1354–1365.
66. **Woolford, Jr., J. L., and J. R. Warner.** 1991. The ribosome and its synthesis, p. 587–626. *In* J. R. Broach, J. R. Pringle, and E. W. Jones (ed.), The molecular biology of the yeast *Saccharomyces*: genome dynamics, proteins synthesis and energetics. Cold Spring Harbor Laboratory Press, Cold Spring Harbor, N.Y.